Norunn Krokeide

Modeling of Saturation and Cross-coupling in a 6-phase IPMSM

Master's thesis in Energy and Environmental Engineering
Supervisor: Prof. Roy Nilsen
February 2024

□ NTNU
Norwegian University of
Science and Technology

Norunn Krokeide

Modeling of Saturation and Cross-coupling in a 6-phase IPMSM

Master's thesis in Energy and Environmental Engineering
Supervisor: Prof. Roy Nilsen
February 2024

Norwegian University of Science and Technology
Faculty of Information Technology and Electrical Engineering
Department of Electric Energy

NTNU
Norwegian University of
Science and Technology

Acknowledgments

Abstract

Accurate modeling of the relation between stator currents and flux linkages in Permanent Manget Synchronous Motors is essential to achieve the best possible control systems. Precise motor models and parameters are especially valuable in the context of sensorless control, where certain algorithms rely on model equations to estimate rotor position. Here, the nonlinearity caused by saturation and cross-coupling phenomena must be included. This project aims to analyze and model the saturation and cross-coupling in a 6-phase IPMSM. Another objective is to further develop nonlinear models of the flux linkages as function of stator currents, by studying a paper with results from comparable tests.

Constant-speed tests of a 6-phase IPMSM are done, applying d- and q-axis current references manually, and this way mapping flux linkages to a range of stator currents in the dq-reference frame. There is not much saturation in the results, but there is some cross-coupling on the d-axis flux, though it is difficult to discern any trends here. There is also some cross-coupling on the q-axis, but very small. The lab results are also curve fitted to several nonlinear polynomial models deduced in previous thesises. A study is then done of the data of a previously conducted paper, analyzing saturation phenomena and developing new more detailed nonlinear flux linkage models that capture the differential inductances. These are fitted to the conducted lab data, which results in a good fit, and it is found that basing the models on curve fits to differential inductances could be a promising approach for future work. Generally, the functions model the flux linkage on the q-axis more precisely than the d-axis. It is discussed that there possibly has been variations on the PM flux on the d-axis, because of saturation and cross-coupling effect, affecting the results. It is recommended that the PM flux variation should be modeled in further work. A limitation to the study is the narrow range of applied currents in the conducted lab tests, due to limitations on the inverter output voltages.

Sammendrag

Nøyaktig modellering av forholdet mellom stator strømmer og flux i en Permanent Magnet Synkronmotor er avgjørende for å oppnå best mulig motorstyring. Presise motormodeller og -parametre er spesielt verdifullt i konteksten av sensorløs styring, hvor flere algoritmer baserer seg på modell-likninger for å estimere rotorposisjonen. Her må ulineariteten forråsaket av magnetiske metning- of krysskoplingsfenomener være inkludert. Denne oppgaven har mål om å analysere og modellere magnetisk metning og krysskopling i en 6-fase IPMSM. Et annet mål er å utvikle ulineære modeller av flux som funksjon av stator strømmer, gjennom å studere en artikkel som har resultater fra sammenliknbare tester.

Tester med konstant hastighet av en 6-fase IPMSM blir gjort, hvor strømreferansene på d- og q-aksen settes manuelt, og på den måten blir flux kartlagt for en rekke statorstrømmer. Resultatene viser lite magnetisk metning, men det er noe krysskopling på d-aksen, selv om det er vanskelig å observere en trend i krysskoplingen. Det er også litt krysskopling på q-aksen, men minimalt. Resultatene fra lab blir også kurvetilpasset til flere ulineære polynomer. Deretter blir dataene fra en eldre artikkel ananlysert med tanke på magnetisk metning og krysskopling, og de blir brukt til å utvikle nye ulineære flux-modeller som fanger tendensene i de differensielle induktansene i dataene i artikkelen. Dataene fra lab blir så kruvetilpasset de nye modellene, som gir gode resultater og viser at det kan være en god fremgangsmåte for videre arbeid å basere modellene på differensielle induktanser. Jevnt over klarer modellene å modellere flux bedre på q-aksen enn på d-aksen. Det kan være at variasjoner i permanent mangetenes flux, på grunn av magnetisk metning og krysskopling, har påvirket resultatene på d-aksen. Flux variasjoner fra permanent magnetene er et relevant spørsmål som med fordel kan modelles i videre arbeid. En begrensning i studien var at spekteret at statorstrømmer i lab var relativt lite, på grunn av begrensninger i spenning fra inverterne.

Table of Contents

Abbrevations

AC Alternating Current

DC Direct Current

IM Induction Machine

$IPMSM$ Interior Permanent Magnet Synchronous Motor

PM Permanent Magnet

$PMSM$ Permanent Magnet Synchronous Motor

PWM Pulse-Width Modulation

$rmse$ Root mean square error

$SPMSM$ Surface Mounted Permanent Magnet Synchronous Motor

VSI Voltage Source Inverter

List of Symbols

$\mathcal{F}$ Magnetomotive force (MMF)

$\mathcal{P}$ Magnetic permeance

$\mathcal{R}$ Magnetic reluctance

μ_0 Magnetic permeability of vacuum

μ_r Magnetic permeability relative to vacuum

ω_n Nominal angular speed

ϕ Magnetic flux

ψ Magnetic flux linkage

τ Torque

θ Rotor angle

ε Electromotive force (EMF)

ϑ Phase shift between winding sets

B Magnetic flux density

B_r Remanence

H Magnetic field strength

L	Inductance
L_{dd}	Self-inductance on d-axis
L_{dq}	Cross-coupling inductance
L_{qd}	Cross-coupling inductance
L_{qq}	self-inductance on q-axis
n	Motor rotational speed in p.u.
p	Number of pole-pairs
x	Reactance
x_d	d-axis reactance
x_q	q-axis reactance
x_σ	Leakage reactance

Lower index

01	01-axis in rotating 01-02 space
02	02-axis in rotating 01-02 space
α	α-axis in stationary 2-phase system
β	β-axis in stationary 2-phase system
a	phase a
b	phase b
c	phase c
d	d-axis in rotating dq-space
e	electromagnetic
L	load
q	q-axis in rotating dq-space
s	stator
$z1$	z1-axis in rotating z1-z2 space
$z2$	z2-axis in rotating z1-z2 space

1 Introduction

This thesis is a continuation of a specialization project thesis delivered in January 2023[1], and is to an extent also a continuation of the work done in several previous Master's projects at NTNU, especially the work of Øyvind Sommer Klyve (2021)[2]. In the specialization project, simulations of an IPMSM with and without cross-coupling were done and analyzed. Some of the background description in this chapter is taken from the specialization project thesis [1]. In addition, this thesis follows some of the work done in the PhD thesis of Aravinda Perera (2023)[3], and several models are taken from it.

1.1 Project motivation

Industrialization and the shift away from fossil fuel reliance toward more sustainable energy solutions have in recent years driven an increased demand for electrical motors. As their adaptation across various industrial sectors, ranging from heavy industrial machinery to automotive and consumer appliances, have increased, so has the market's requirements with regards to efficiency, reliability, fast performance and low maintenance.

The Permanent Magnet Synchronous Motors (PMSMs) are one type of electrical motors that are performing with very high efficiencies and low weight compared to their power ratings[1]. As a result, PMSMs are increasingly being used in the aforementioned industrial sectors and have been capturing a substantial part of the electric motor market for many years. The demand for PMSMs is also expected to increase significantly.

As a substantial part of the world´s electric energy is converted in electric motors, and by that in PMSMs, even small increases in efficiency and reliability would be highly beneficial not only to customers but also to the environment and society. One approach that has resulted in substantial improvements in reliability, efficiency and control performance is the development of sensorless control systems.

Efficient control systems of motors rely on feedback of the motor position in order to function optimally. In sensorless control, this is not provided by a physical sensor or encoder, but rather by observers which use motor measurements and model parameters to estimate the position. This reduces the overall amount of electronics, leading to lighter, more cost-effective and easier to maintain systems. Extensive research and improvements on the implementation of sensorless control in motors have been conducted, and while the method is now widely accessible and the standard for many applications, [4], the technology is still evolving.

Generally, sensorless control is categorized into model-based and high-frequency signal injection-based methods, each having their advantages and limitations. Model based control algorithms rely on modeling the motor mathematically, as they estimate the back-EMF or flux linkage, and then calculate the rotor position from this, as well as the motor model equations. The rotor position is then fed into the control system. Here, accurate identification of motor parameters and models is essential, as the observers calculating rotor position need to deliver very precise estimates.

An essential part to the motor models is related to the electromagnetic induction and flow of flux through the motor. This includes the relation between applied currents and flux linkages, which is rather complex and depends on motor design. The magnetic cross-coupling effect, which is linked closely to magnetic saturation, and where the current on each axis produce flux linkages on the other axis, is one of the difficulties to model the motor correctly. Challenging operational conditions, as encountered in industrial settings, demand that the motors perform very well also in the saturated region[5], where the magnetic flux behaviour changes and affects the motor parameters. This means that it is necessary to have highly precise models and parameters in this region.

Saturation is a well-known physical phenomenon, and saturation and cross-coupling has been extensively studied in previous research on electric motors, including PMSMs, due to its significant impact on performance and control. Excessive saturation results in increased current demand per torque output, which is not desirable. However, significant magnetization of the motor may often be necessary to obtain the optimal operational efficiency.

Next, there are naturally variations in the magnetic fields, currents, back emf etc. when the dimensions, geometry or materials of the motor are changed. Consequently, the saturation and cross-coupling effects differs among various motors. It is therefore interesting to study these effects more closely for a given motor, in the context, but not with the aim, of improving the motor operation. The ultimate goal would be to understand the characteristics of the cross-coupling and saturation, model it and explain why and where it would occur. This would clearly contribute to further development and knowledge in the field.

1.2 Project objective

The overall objective of this thesis is to explore the saturation and cross-coupling effects in an 6-phase IPMSM, facilitating the implementation of sensorless control further on. In the thesis of Klyve (2021)[2], several different functions were presented that modeled the flux linkage to stator current relation in the dq-reference frame, including cross-coupling effect and saturation. It was also shown that linear functions were not sufficient for their finite element motor model results.

Therefore, one of the objectives of this work is to develop new non-linear flux linkage models and evaluate these, along with existing non-linear models, by applying them on lab data. In addition, there is an intention to identify possible saturation and cross-coupling phenomena in the obtained lab data, and analyze these against comparable data from previously published studies.

To obtain data to analyse, an IPMSM will be evaluated at local lab facilities at the Department of Electric Energy, NTNU. A constant-speed identification method will be used to map the flux linkages against the applied stator currents.

Based on the work conducted in previous thesises and literature, new motor models will be proposed, evaluated and fitted to the lab data. Qualitative data presentation will be prioritized, to facilitate meaningful data analysis and extraction, as there is also an intention to identify possible saturation and cross-coupling phenomena.

Below, the main objectives of this work is summarized:

- Perform lab tests on a 6-phase IPMSM and measure the flux linkages against currents

- Apply existing non-linear models to the obtained data

- Analyze saturation and cross-coupling phenomena in the lab data and data from a previously conducted study

- Refine existing models and develop new ones to better fit the data, while thoroughly evaluating their performance

1.3 Outline of thesis

Chapter 2 introduces the main theoretic concepts and equations that are fundamental to this thesis, including electromagnetic theory and an overview of the PMSM. The saturation and cross-coupling effect will be thoroughly presented here.

Chapter 3 puts forward the method and execution of lab tests. The results are presented and there is done analysis of whether the results are credible, and some discussion on important findings in the results.

Chapter 4 revolves around the study of an IPMSM by Stumberger et al. (2003) [6]. Here, several flux linkage model functions are tested to fit the digitized study data, and saturation and cross-coupling phenomena was analyzed.

In chapter 5, the results from conducted IPMSM tests were fitted to a model developed in chapter 4.

Chapter 6 includes the discussion of the overall results, methods and findings. Some hypothesises of saturation and cross-coupling effects were put forward.

Chapter 7 concludes the thesis, including main findings and limitations.

2 Theory

There are some definitions, models and general theory on electromagnetism that is needed for understanding the analysis in subsequent chapters. This is presented in the current chapter. Some of the theory in chapter 2.2 and 2.4 regarding PMSMs are reproduced from the specialization project thesis written ahead of this master's thesis [1].

2.1 Electromagnetism and magnetic materials

The magnetic flux density, B, in a material is defined by the applied magnetic field strength H and the permeability of the material, μ, as seen in equation 1. The permeability of a material is a value describing the material's response to an applied magnetic field. Materials with high permeability, e.g. iron, obtain a higher magnetic flux density than materials with low permeability, like air or other insulation mediums, for the same applied magnetic field strength.

$$B = H\mu = H\mu_0\mu_r \tag{1}$$

Another important term is magnetic saturation. This is a well known phenomena which occurs when there has been applied so large of an magnetic field that the magnetic material cannot be magnetized much more. This is best described by equation 1, where the permeability stops being constant and the curve is no longer linear. This is shown in the well-known b-h or hysteresis curve, in figure 1. Again, B is the magnetic flux density in the material and H is the field strength of the applied magnetic field [7]. The understanding of this phenomena is that the many small magnetic domains, which the magnetic material consist of, align themselves with the direction of the outer magnetic field that is applied. At a certain point, the majority of these small magnetic domains point in the same direction, and it is simply not possible to align many more domains and by that magnetize the material much more.
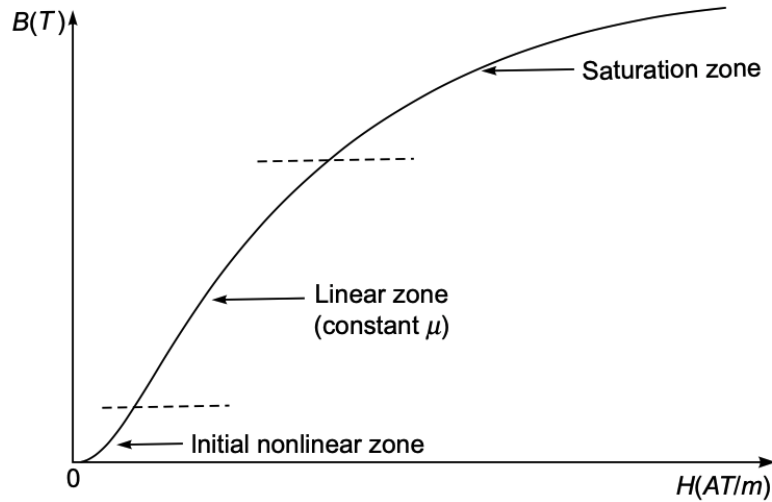

Figure 1: Typical magnetization curve for ferromagnetic material, from [7]

The magnetic flux, ϕ is the integral of magnetic flux density or magnetic field over a surface, shown in equation 2. Flux linkage, ψ, is defined as the flux that is linked by all the windings in a coil it passes through [8], and is defined in equation 3.

$$\phi = \int_s \vec{B}\vec{ds} \tag{2}$$

$$\psi = N \cdot \phi \tag{3}$$

Another essential term is the magnetomotive force (MMF), $\mathcal{F}$, which is the force or source driving the magnetic flux. Next, reluctance, $\mathcal{R}$, is the relation between the MMF and the resulting flux in a magnetic circuit, as seen in equation 4, and can be seen as the resistance the magnetic flux sees flowing through a magnetic material. The inverse of reluctance is permeance, $\mathcal{P}$, which is closely related to the term permeability presented above. Equation 4 is analogous to Ohm's law in electrical circuits, and the electrical terms of resistance, electromotive force (EMF) and

current. Returning to the phenomena of saturation; when a material is saturated, the resulting flux linkage from an applied magneto-motive force is decreased. This can also be seen as the reluctance increasing in the magnetic circuit, as seen in 4.

$$\mathcal{F} = \phi \cdot \mathcal{R} = \frac{\phi}{\mathcal{P}} \tag{4}$$

There are some laws that must be followed when studying magnetic circuits. Kirchhoff's voltage law can be applied, where the sum of MMF sources and MMF drops are equal in a magnetic circuit. Next, the flux is continuous through a closed circuit, meaning the sum of flux into a node is same as out, which can be related to Kirchhoff's current law in electrical theory. However, a very important difference between electrical and magnetic circuits is that the flux leaks outside the magnetic circuit, and one therefore has to include this in the calculations. Also, reluctance does not dissipate energy the way that electrical resistances do.

The magnetomotive force in a magnetic circuit is naturally proportional to the applied magnetic field, which can also be understood though observing the equations presented above. Note that the magnetic flux always will go through the path of least reluctance, the same way an electric current does with resistance. Another way to express the reluctance of a magnetic circuit or part of a circuit, which is used when handling motor models, is to determine the effective air gap. The air gap between stator and rotor represents a large magnetic reluctance, as air has very low relative permeability, close to unity.

$$\varepsilon = -\frac{d\psi}{dt} = -N\frac{d\phi}{dt} \tag{5}$$

$$\varepsilon = N\frac{d\phi}{di}\frac{di}{dt} = L\frac{di}{dt}$$
$$L = N\frac{d\phi}{dt} = \frac{d\psi}{di}$$
$$\psi(i) = Li \tag{6}$$

The phenomena of electromagnetic induction is generally described by Faraday's law, presented in one of its many forms in equation 5. Induction occurs when a magnetic field is applied on a winding. Lenz's law states that there will be induced a current in that coil working against the change in the applied field. This current corresponds to an induced electromotive force, given in volts. It is not necessary to include the negative sign, as long as one is aware of the direction of flux and current. When this equation is expanded, and the inductance is introduced, the relation between current and magnetic flux linkage in a winding can be deduced, as seen in 6. This is a very useful equation further on. Lastly, as $X_L = 2\pi f \cdot L$, and the base values are chosen such that the per unit values are equal, x can also be referred to as the inductance, and the symbols are often used interchangeably.

2.1.1 Permanent Magnet properties

An essential property of a permanent magnet (PM) is its very high coercivity. This means that it will take a very strong external magnetic field to demagnetize it. Another important property is its remanence, which is the largest flux density produced by the PM itself, and is denoted B_r. If the PM should produce this, it would require being surrounded by a material of infinite permeability, leading the flux linkage between north- and south-pole with no reluctance, but this is not the reality. Here, it is important here to note that the magnetic flux density leaving the magnet is dependent on its surroundings. It will follow the B-H curve of the PM material, but the point on the curve is determined by the surroundings.

$$\phi = \phi_r + P_m\mathcal{F}_m = B_rA_m + \frac{1}{\mathcal{R}_m}H_ml_m \tag{7}$$

$$B_m = B_r + \mu_0\mu_rH_m$$
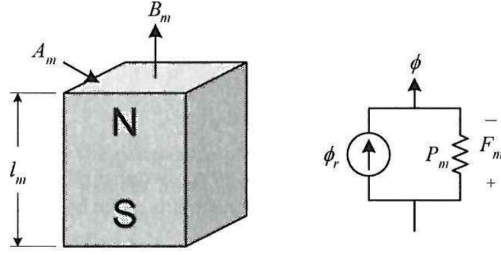$$\phi = B_mA_m \tag{8}$$

Figure 2: Magnetic circuit of a PM, taken from [8]

The magnetic circuit equivalent of a PM is presented in figure 2 from [8], and the corresponding equation 7. There is an assumption that the PM is evenly magnetized over the cross-section. In this equivalent, there is a magnetic flux source, corresponding to a current source in an electrical circuit, and an inner reluctance, which electric equivalent is a resistance, which is placed in parallel with the source. Note that the magnetic flux density out of the PM, B_m is lower than the remanence B_r, which is provided by the parallel reluctance. This reluctance has a flux equal to the so called magnet leakage permeance, $\mathcal{P}_m$, times the MMF.

2.2   The Permanent Magnet Synchronous Machine

Like other electric motors, the Permanent Magnet Synchronous Motors convert between electric and mechanic energy, where the electric energy is applied through a voltage in a set of stator windings, and the mechanical energy is consumed by a load connected to the axle of the rotor. Synchronous machines are characterized by the fact that the magnetic flux vector generated by the stator currents rotates synchronously with the rotor. The PMSM is similar to other synchronous machines, but has permanent magnets in the rotor instead of rotor windings, where torque is generated by applying a magnetic field on the magnets. This construction makes it possible to make motors with smaller losses and high speeds and torques relative to their weight [9]. An important aspect is that since there are no windings in the rotor, there are also no copper losses here. The permanent magnet can also be cheaper than an electromagnet of coils, depending on the magnet material, size and number of coil windings.
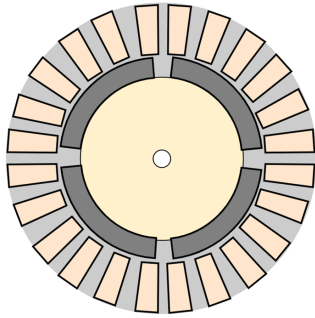
(a) Illustration of surface mounted PMSM with 4 poles
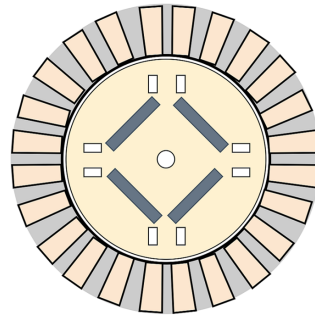
(b) Illustration of IPMSM with 4 poles and tangential rotor configuration

Figure 3: Surface mounted and interior PMSMs illustrated, from [1]

There are two types of PMSMs, that only differ by the placement of the permanent magnets. In the Surface Permanent Magnet Synchronous Motor (SPMSM), as shown in 3a, the magnets are placed on the surface of the rotor. In this configuration there will be both an air-gap between the individual rotor mounted magnets and also an air-gap between these magnets and the stator. The other possible placement of the permanent magnets is inside the rotor, giving the Interior Permanent Magnet Synchronous Motor (IPMSM), shown in 3b. In the IPMSM, the air-gap is much smaller and the mechanical strength higher, enabling safe operations at higher rotor speeds [10].

Another important difference is that while there is no or very little saliency in a SPMSM, there is significant saliency in an IPMSM. Magnetic saliency in a motor means that the reluctance is not distributed evenly along the air-gap, and represents the difference between the two axes in terms of reluctance or inductance. In other words, the air-gap and inductance is the same for all axes on an SPMSM, and varies on the axes of an IPMSM.

PMSMs are fed with a 3-phase voltage (3-phase PMSM) or a 6-phase voltage (6-phase PMSM), usually from an inverter that is controlled by PWM technique or otherwise. The two voltage components in the dq-reference system, which are from definition independent of each other, are the control signals [11]. The drive would consist of a voltage source, either an ac voltage source or a dc source, going into the inverters.

The number of slots and conductors are chosen in the motor design such that the resulting magnetic field waveform that is set up by the stator voltage is as close as necessary to sinusoidal [11]. There is also other concerns in the design, as cost, weight and losses, and there will always be a trade-off between different advantages of design choices. Still, the stator voltage induced magnetic field is usually some sort of disturbed sinusoidal waveform.

2.3   Reference frames

A rotating two-phase reference frame that rotates synchronously with the rotor is preferred instead of a stationary reference frame when the motor model will be presented next. Using established transformation equations, the sinusoidal three-phase or 6-phase currents in the stator can be represented as dc-currents, which is much easier to handle. Here, the two currents will be orthogonal to each other in the plane and therefore independent of each other. Using a rotating reference frame also makes the calculations including the rotor angle much simpler, as it follows the reference frame.
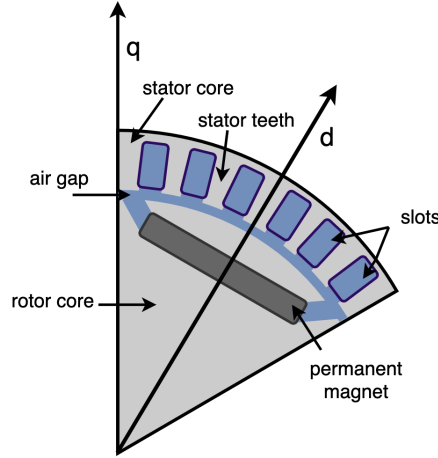
2.3.1   The dq-reference frame

Figure 4: d- and q-axis on 6-pole IPMSM illustration

First, for three-phase windings, the rotating dq-reference frame should be introduced. The two axes in this reference system are called the direct axis (d-axis), and the quadrature axis (q-axis). The direct axis in an IPMSM is defined in the direction with the highest magnetic reluctance, and the quadrature axis is shifted 90 electrical degrees from this. As the permanent magnet is made of a low-permeability material, the d-axis follows the flux vector of the permanent magnet, as illustrated in figure 4. The q-axis goes between the permanent magnets, where there is lower reluctance. The rotor angle θ, which is the angle between the α-vector and the rotor position, is now equal to the angle between the d-axis and the α-vector.

Now, consider a three-phase setup. The Clarke-transformation is used to transform three-phase currents into two-phase currents, as seen in equation 9. The transformation to a rotating reference frame is done through the Park-transformation, as can be seen in equation 10.

$$i_\alpha = \frac{2}{3}i_a - \frac{1}{3}i_b - \frac{1}{3}i_c$$
$$i_\beta = \frac{1}{\sqrt{3}}(i_b - i_c)$$

(9)

$$i_d = i_\alpha \cos\theta + i_\beta \sin\theta$$
$$i_q = -i_\alpha \sin\theta + i_\beta \cos\theta \tag{10}$$

2.3.2 Reference frame for 6-phase systems

Next, consider the 6-phase system, which is applied in the control system of the lab setup introduced later on. Again, it is useful to have a rotating reference frame with dc-values, but the six phases cannot be transformed into the dq-frame only. The six winding phases are therefore transformed into the three d-q, z1-z2 and 01-02 subspaces, which are defined to be orthogonal and independent of each other. This is called the Single Synchronous Reference Frame (SSRF) [3].

$$S_k(\omega t) = \begin{bmatrix} \cos k\omega t \\ \cos k(\omega t - \vartheta) \\ \cos k(\omega t - 4\vartheta) \\ \cos k(\omega t - 5\vartheta) \\ \cos k(\omega t - 8\vartheta) \\ \cos k(\omega t - 9\vartheta) \end{bmatrix} \tag{11}$$

$$T_{ss}^r(\vartheta) = \begin{bmatrix} S_1(\vartheta, 0) \\ S_1(\vartheta, \frac{\pi}{2}) \\ S_5(-\vartheta, 0) \\ S_5(-\vartheta, \frac{\pi}{2}) \\ S_3(0, 0) \\ S_3(0, \frac{\pi}{2}) \end{bmatrix} \tag{12}$$

$$\begin{bmatrix} u_d \\ u_q \\ u_{z1} \\ u_{z2} \\ u_{01} \\ u_{02} \end{bmatrix} = [T] \cdot \begin{bmatrix} u_{a1} \\ u_{b1} \\ u_{c1} \\ u_{a2} \\ u_{b2} \\ u_{c2} \end{bmatrix} \tag{13}$$

$$\begin{bmatrix} i_d \\ i_q \\ i_{z1} \\ i_{z2} \\ i_{01} \\ i_{02} \end{bmatrix} = [T] \cdot \begin{bmatrix} i_{a1} \\ i_{b1} \\ i_{c1} \\ i_{a2} \\ i_{b2} \\ i_{c2} \end{bmatrix} \tag{14}$$

The vector defined in equation11, presented in a study by Zhao (1995) [12], is the first step in the transformation to SSRF. More specific, these vectors go into the transformation matrix in 12. This matrix can be used to obtain the d, q, z1, z2, 01 and 02 voltages and currents from the 6-phase voltages and currents, applying equations 13 and 14. Here, ϑ is the phase shift between the two three-phase winding sets of the motor and k represents the order of the harmonics [12]. The d-q surface is defined to include the fundamental component, and therefore has k equal to one. The z1-z2 surface is defined with k equal to five, and the 01-02 surface has k equal to three, and this results in the three spaces being orthogonal. ωt was equal to zero and ninety degrees in d-q and z1-z2 subspaces, and zero and thirty degrees in the 01-02 subspace. This is provided in further detail in Zhao (1995) [12].

$$S_3(0,0) = \begin{bmatrix} 1 & 0 & 1 & 0 & 1 & 0 \end{bmatrix} \qquad\qquad S_3(0, \frac{\pi}{2}) = \begin{bmatrix} 0 & 1 & 0 & 1 & 0 & 1 \end{bmatrix} \tag{15}$$

Note next that the 01-02 subsystem will be excluded in the motor calculations. The reason for this is the assumption that the sum of the three phase currents in each set of windings is zero. It is well known from electrical theory that is the case for three shifted sinusoidal signals. Observing the vectors presented in 15, as well as the equation 14,it is clear that as long as this assumption holds, the 01-02 subspace currents are also zero.

$$f_d = \frac{f_{d1} + f_{d2}}{2} \qquad\qquad f_q = \frac{f_{q1} + f_{q2}}{2} \tag{16}$$

$$f_{z1} = \frac{f_{d1} - f_{d2}}{2} \qquad\qquad f_{z2} = \frac{f_{q1} - f_{q2}}{2} \tag{17}$$

In some cases it is useful to use a Double Synchronous Reference System (DSRF), for instance when there are two separate supplies for the two three-phase winding sets, that have their own PWM-controlled inverters. Here each three-phase group is transformed from three-phase to the two-phase dq-frame according to the transformations in the precious chapter. The transformation from DSRF to SSRF is presented in equations 16 and 17, from [3]. The transformation from SSRF to DSRF can be deduced from these same four equations as well.

2.4 The PMSM model

The following equations, starting with 18, 19, represent a mathematical model that describes the inner workings of the PMSMs [11]. Upper case parameter symbols are in actual values, while lower case parameter symbols are in per unit. Both interior and surface mounted permanent magnet machines can be described by this model, but as noted in 2.2, where IPMSMs have magnetic saliency in the rotor, with $L_d < L_q$ and $\mathcal{R}_d > \mathcal{R}_q$, PMSMs have not, resulting in $L_d = L_q$ and a simpler model. The model includes stator voltage, stator current and flux linkage in the q- and d-axes presented previously, as well as stator resistance r_s, rotor speed n and nominal angular motor speed ω_n.

$$u_d = r_s i_d + \frac{1}{\omega_n}\frac{d\psi_d}{dt} - n\psi_q \tag{18}$$

$$u_q = r_s i_q + \frac{1}{\omega_n}\frac{d\psi_q}{dt} + n\psi_d \tag{19}$$

The voltage equations have three terms on the right hand side, the first being the stator winding copper losses $r_s i_d$. This resistance is very small and usually of little significance compared to the other terms, but it is also known to be temperature-dependent. The second term is the part of the stator voltage proportional to the flux derivative, relating to Faraday's law. The back-EMF is also included in the model, in the last term which is proportional to both flux linkage and speed.This back-EMF is the voltage the rotation generates when the stator coils induce current to oppose the flux variations from the rotor PMs. Here Lenz' law is applied.

$$\psi_d = \psi_{dm} + \psi_m \tag{20}$$

$$\psi_d = i_d x_d + \psi_m \psi_q = i_q x_q \tag{21}$$

Another flux parameter will be important and should be introduced, namely ψ_{dm}. Since the d-axis is aligned with the PM, and the magnetic flux linkage from the PM is purely on the d-axis, it is useful to separate the part of the d-axis flux caused by the stator winding currents and the part set up by the PM's magnetic field. These two parts correspond to ψ_{dm} and ψ_m respectively in equation 20. The flux on the d- and q-axis induced by stator currents is also represented by the same axis current times a reactance, assuming a linear relationship for now. An important observation is that when i_d is negative, the current-induced part of the d-axis flux, $\psi_{dm} = \psi_d - \psi_m$, will work in the opposite direction as the flux from the PM in the d-axis. Therefore, field weakening in a PMSM is applied by increasing the negative d-axis current. Field weakening is needed when the speed is accelerated above its nominal value, and the stator voltage has to be maintained within certain limits with regards to the inverter, typically.

$$\tau_e = \psi_d i_q - \psi_q i_d$$
$$\tau_e = \psi_m i_q - (x_q - x_d) i_d i_q \tag{22}$$

Next, the electromagnetic motor torque, τ_e, follows equation 22 and has two separate terms. The first term is the magnetic torque, which is caused by the interaction of the rotor magnetic field from the PMs with the stator windings. From physics theory it is known that electric charges, coils conducting current and magnetic materials will experience a force when there subjected to a magnetic field. The second term is the reluctance torque due to rotor saliency, which is visible as the term depends on $x_q - x_d$. Since the inductance is not distributed evenly, meaning there is magnetic saliency, the rotor will move toward the position that minimizes the reluctance as seen from the stator flux. When the rotor is forced to move so the rotor and stator flux vectors are aligned, there is produced torque. Generally, since the q-axis is the main torque producing axis, it is important to control the q-axis current. The d-axis current mainly controls the field weakening and does not produce much torque, though this depends on the motor saliency. This is visible in figure 5, where the two terms of equation 22, as well as the sum, are plotted for different current vector angles φ.
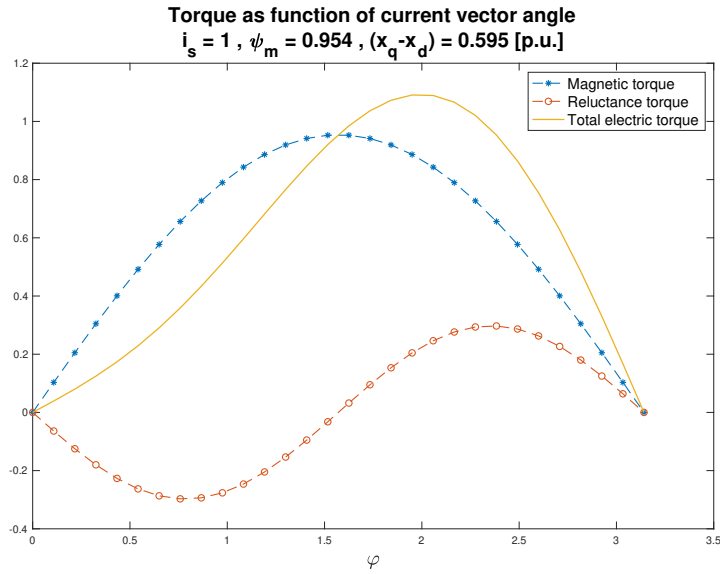

Figure 5: Electric torque with variation in current vector angle

$$T_m \frac{dn}{dt} = \tau_e - \tau_L \tag{23}$$

Lastly, the rotor speed is determined by the torque balance on motor and load, as is understood through Newton's second law of rotation, applied in 23. Here, T_m is simply a constant from the base-value calculations and motor inertia.

2.4.1 The motor model in a 6-phase reference frame

Since a 6 phase motor is to be studied, the dq-reference frame model is not sufficient, the model must be extended to include the d-q,z1-z2 and 01-02 reference frame. As explained in the previous chapter, the 01-02 subspace currents are zero as long as the three-phase currents in each winding set sums to zero. As this is the case, also the 01-02 subspace flux linkages and voltages become zero. Otherwise, the equations in the dq-subspace are the same as presented in the general model above.

$$
\begin{bmatrix} u_d \\ u_q \\ u_{z1} \\ u_{z2} \end{bmatrix} = r_s \cdot \begin{bmatrix} i_d \\ i_q \\ i_{z1} \\ i_{z2} \end{bmatrix} + \frac{1}{\omega_n} \cdot \begin{bmatrix} \psi_d \\ \psi_q \\ \psi_{z1} \\ \psi_{z2} \end{bmatrix} + n \cdot \begin{bmatrix} -\psi_q \\ \psi_d \\ \psi_{z2} \\ -\psi_{z1} \end{bmatrix} \tag{24}
$$

$$ \psi_d = x_d i_d + \psi_m \qquad\qquad\qquad \psi_q = x_q i_q \tag{25} $$
$$ \psi_{z1} = x_{s\sigma} i_{z1} \qquad\qquad\qquad \psi_{z2} = x_{s\sigma} i_{z2} \tag{26} $$

$$ x_d = x_{md} + x_{s\sigma} \qquad\qquad\qquad x_q = x_{mq} + x_{s\sigma} $$

The motor model in SSRF is presented in the equations in 24 and the corresponding flux linkage equations. The d- and q-axis reactances are separated into a stator leakage reactance, pertaining to the flux that does not cross the air-gap, but simply goes from one PM pole to another in the air-gap, and a magnetizing reactance, pertaining to the flux that crosses the air-gap into the stator teeth and yoke. Note also that the flux linkage in the d-q subspace includes the total d- and q-axis reactance, while the z1-z2 subspace is equal only to the flux linkage that leaks through the air gap, which does not produce torque. One property of the z1-z2 subspace is that it is not related to electromechanical energy conversion [12], and this simplifies the calculations greatly. Although present in the control system, the z1-z2 subspace will not be considered when the cross-coupling and saturation is studied further in this thesis.

2.5 Magnetic fields in the motor

As explained previously, the magnetic field waveforms set up by the stator windings are ideally sinusoidal. The direction of the magnetic field at each moment is decided by the current magnitudes in each winding, and the right hand-rule. This is illustrated in figure 6, which is copied from the TET4120 Electric Drives course compendium [11], with some minor changes. Here, there are only two poles, and only one phase with currents, with resulting magnetic field. The field in this illustration has a squared shape along the air gap, but as explained previously, the design and number of slots determines this shape. The field lines will then be distributed in the rotor, air gap, stator teeth and yoke.
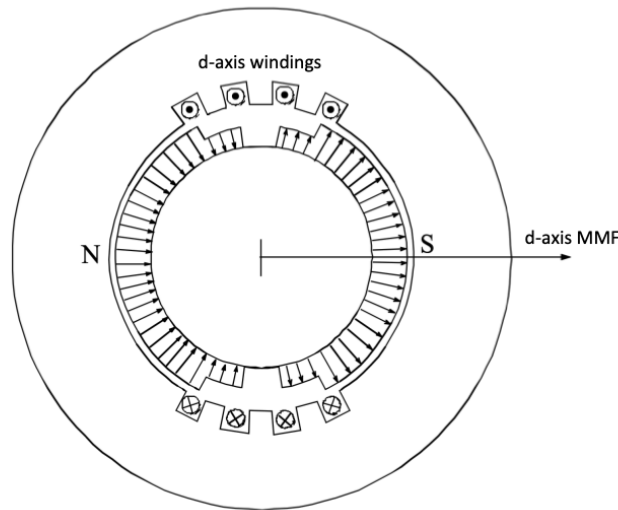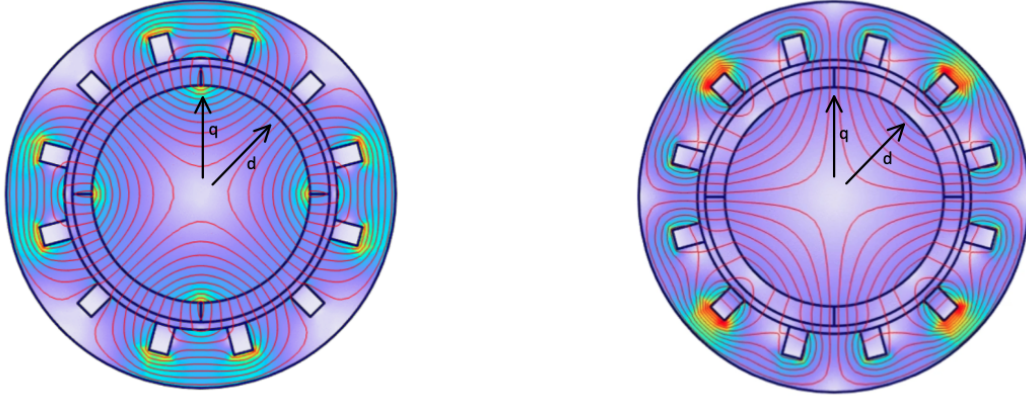

Figure 6: Magnetic field set up by a set of windings, from TET4120 course compendium [11]

(a) 4 pole IPMSM with fields from PM in d-axis

(b) 4 pole IPMSM with q-axis current

Figure 7: Illustration of magnetic field in IPMSM, taken from [13]

In figures 7b and 7a, the cross-section of an IPMSM including magnetic field lines is visualized. These illustrations are taken from slides by R. Nilssen [13] with small changes, and display a motor that will not be studied further, but is only used to illustrate the placement of magnetic fields. This motor has 4 poles, meaning that the geometry looks a little different, with four set of magnetic field lines and 45 mechanical degrees, instead of six set and 30 degrees in a machine with 3 pole-pairs which will be studied later, but the principles remain the same. The first diagram, figure 7b, shows the magnetic field when there is only flux from the PM, meaning there is no q-axis or d-axis current, only magnetic field from the PM, following the d-axis. The second diagram, figure 7a, shows the field when there is only q-axis current applied. The motor is at the same rotor position in these two, but the flux vector is aligned with the d-axis in 7b and the q-axis in 7a.

$$\theta_{electrical} = \theta_{mechanical} * p \tag{27}$$

It is important to note that the two fields are 90 electrical degrees shifted, or are perpendicular to each other, as understood through equation 27, where the relation between electrical and mechanical degrees in a motor is presented. Another important observation is that the two fields will be overlapping.

2.6 Saturation and Magnetic Cross-coupling effect in IPMSMs

The phenomena of saturation and cross-coupling are both very important to the motor modeling, and they are also closely related. Saturation and cross-coupling may occur at different places in the motor, depending on the motor design and applied currents.

2.6.1 Saturation

The general magnetic saturation effect was explained thoroughly in chapter 2.1. Saturation is very much present in IPMSMs, as long as there is sufficient total flux. The stator core and teeth are made of iron, a ferromagnetic material, and will be saturated. Since the permanent magnets each set up their own magnetic field, they also contribute to saturation, in addition the induced magnetic field from the applied stator currents and the back-EMF. The result is that IPMSMS very much are magnetized also at no load, i.e. no stator current. The degree depends on the motor design, but regardless, the motors should be magnetized a lot in order to function optimally. One effect of this is that they then become more sensitive to magnetic fields being applied, as they are farther up the bh-curve. Note also that as long as one operates with negative d-axis fluxes, and ψ_{dm} consequently has the opposite direction as ψ_m as explained above, the total magnetic field is smaller, and this will move the motor toward lower saturation.

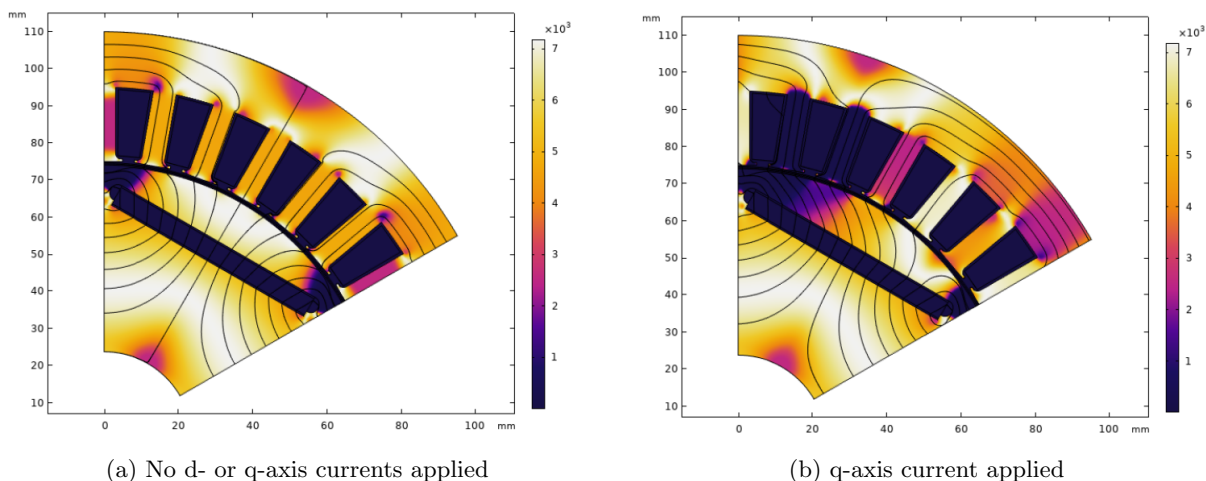(a) No d- or q-axis currents applied   (b) q-axis current applied

Figure 8: Relative magnetic permeability in section of IPMSM, from Klyve (2021) [2]

2.6.2 Cross-coupling

There was an assumption in the standard model presented in equations 21 that the two dq-axes currents only produce flux on their own axes, giving linearity. However, previous studies have proved that the d- and q- stator currents affect the magnetic flux linkage in the other axis [6] [14] [2].

The magnetic flux path goes through the rotor iron, the PM, the air-gap, the iron stator teeth and the yoke, saturating the iron when the field is strong enough. The flux in one axis will contribute to saturation of the iron also outside its own axis. In the dq-frame, where there are only two independent axes, this means that the d-axis flux saturates iron along the q-axis, and the opposite. As shown previously in figure 7, the d-and q-axis fields in an IPMSM will be overlapping, therefore affecting the other axis' magnetic flux density and iron magnetization.

This is known as the cross-magnetization effect, cross-coupling magnetic saturation effect or simply cross-coupling effect. The effect is visualised in figure 8, taken from [2]. The plots show the relative magnetic permeability in an IPMSM, calculated numerically with the finite element (FE)-method. As explained from the hysteresis curve in chapter 2.1, the relative permeability decreases when a material is saturated, so the permeability plot is useful to observe saturation. Again, the d-axis is through the PM, and the q-axis is 90 electrical or 30 mechanical degrees shifted. The magnetic flux lines from the PM are visible in figure 8a, where there are no armature currents. The flux lines align with the d-axis, just like in the cross-section plot in figure 7b. What is visible that when q-axis current is applied in figure 8b, there is quite a bit of saturation on both axes.

Some propositions on the saturation phenomena can be done based on existing theory. The highest flux density from the stator windings will likely be in the yoke above the opposite axis, since the axis windings and direction of the axis is 90 degrees on each other. It is visible in figure 7 how the fields of the two axes must overlap and how the field density should be high in the yoke. Based on the direction of the magnetic flux lines, it is a fair assumption that the yoke above the axes is some of the places in the motor that would be most saturated. Also in the cross-section FEM-plot in figure 8, there was clearly higher saturation in the yoke directly on the axes.

The iron in the rotor can naturally also reach saturation when the applied field is strong enough, as seen in 8. Another proposition is that there will be saturation locally in the stator winding slots. Note also that the effective air-gap is smaller on the q-axis, making it prone to saturation. Although the effective air-gap is larger on the d-axis, the iron here is significantly magnetized at no-load because of the PM. This should be registered for the analysis further on.

2.6.3 Saturation and cross-coupling effect on PM

Lastly, one must consider how the PM flux linkage is affected by saturation and cross-coupling. Previously, in equation 8, it was understood that the PM magnetic field is dependent on its surroundings. When the iron on the d- and q-axes is saturated, increasing the reluctance along the path, the flux linkage in the path will decrease, regardless of the excitation source that is the PM. This can be modeled by the relative permeability surrounding the magnet decreasing, leading to a lower PM field in equation 8, or by the fictitious reluctance increasing, leading to a lower flux in equation 7. There is also cross-coupling here, so q-axis currents increase saturation on the d-axis, giving smaller flux linkage from the PM in addition to smaller flux linkage from d-axis stator current if that is applied.

2.7 Modeling the cross-coupling and saturation

As explained previously, standard models of permanent magnet motors assume that the relationship between the current applied and flux linkage in the d- and q-axis is linear, as in 28, where the d- and q-axis reactances x_d and x_q are constant.

$$\psi_{dm} = x_d i_d$$
$$\psi_q = x_q i_q \tag{28}$$

$$\psi_{dm} = x_d(i_d, i_q) \cdot i_d$$
$$\psi_q = x_q(i_d, i_q) \cdot i_q \tag{29}$$

When the cross-coupling and saturation or non-linearity is introduced, this can be done in quite a few different ways. There have been put forward polynomial models of different orders, and exponential models. Both the currents and flux linkages could be chosen as state variables, as shown in 30 and 31 respectively.

$$\psi_{dm} = \psi_{dm}(i_d, i_q)$$
$$\psi_q = \psi_q(i_d, i_q) \tag{30}$$

$$i_d = i_d(\psi_{dm}, \psi_q)$$
$$i_q = i_q(\psi_{dm}, \psi_q) \tag{31}$$

Going forward, current will mainly be used as s.v. in this thesis. Some papers keep to the model in equation 28 above where the same axis current is kept outside, essentially introducing more complex non-constant expressions for the reactances, as seen in 29. There are also examples of models introducing terms that only depend on the other axis current, introducing cross-coupling reactances x_{dq} and x_{qd}, but in order to avoid mix-ups in terminology, these terms will not be used further in the thesis. It can be advantageous to keep all terms dependent on the same axis current, as in equation 28, as the d- and q-axis reactances can be studied more easily, although there are precise models of both types.

2.7.1 Self- and cross-coupling inductances

Some more parameter definitions are needed in addition to the d- and q-axis reactances and inductances x_d, x_q, L_d and L_q. In this thesis the terminology from [6] will be followed; L_{dd} and L_{qq} are called self-inductances and L_{dq} and L_{qd} are called cross-coupling inductances. They are defined in 32, as partial derivatives of the flux linkages. Mutual inductances is also a commonly used term which refers to the same as cross-coupling inductance. These partial derivative expressions can be approximated by the self- and cross-coupling differential inductances, which can be useful if there are mapped results with many steps/datapoints. This approximation of the self-and cross-coupling inductances is showed in equations 33.

$$\begin{bmatrix} L_{dd} & L_{dq} \\ L_{qd} & L_{qq} \end{bmatrix} = \begin{bmatrix} \frac{\partial \psi_d}{\partial i_d} & \frac{\partial \psi_d}{\partial i_q} \\ \frac{\partial \psi_q}{\partial i_d} & \frac{\partial \psi_q}{\partial i_q} \end{bmatrix} \tag{32}$$

$$
\begin{aligned}
L_{dd} &= \frac{\partial \psi_d}{i_d} \approx \left. \frac{\Delta \psi_d}{\Delta i_d} \right|_{i_q = c} \\
L_{dq} &= \frac{\partial \psi_d}{i_q} \approx \left. \frac{\Delta \psi_d}{\Delta i_q} \right|_{i_d = c} \\
L_{qd} &= \frac{\partial \psi_q}{i_d} \approx \left. \frac{\Delta \psi_q}{\Delta i_d} \right|_{i_q = c} \\
L_{qq} &= \frac{\partial \psi_q}{i_q} \approx \left. \frac{\Delta \psi_q}{\Delta i_q} \right|_{i_d = c}
\end{aligned}
\tag{33}
$$

2.7.2 Reciprocal condition

The reciprocal condition, ensuring that a system is conservative, is presented in equation 34 for a model in the dq-reference frame. In simple terms it ensures that no energy is lost, only transferred, and it can be understood by observing the equations for energy stored in a magnetic field. The reciprocal condition demands that the mutual inductances in two coils setting up B-fields that affect each other, are the same.

$$
\begin{aligned}
\frac{\partial \psi_d}{\partial i_q} &= \frac{\partial \psi_q}{\partial i_d} \\
L_{dq} &= L_{qd}
\end{aligned}
\tag{34}
$$

2.7.3 Modeling the PM flux

Next, the saturation and cross-coupling effect on the PM flux has to be addressed. Previously in chapter 2.1, the equivalent of a PM was introduced, a flux source in parallel with a reluctance, which would be equivalent to a coil producing a MMF in series with the same reluctance. Now, it is known from equation 6 that the flux linkages of a coil equals inductance times current through the coil. Therefore, the PM flux is represented by a fictitious current times a fictitious inductance, as seen in the first line of equation 35. In equation 35, the PM flux is also introduced as a variable term. The d-axis reactance is also separated into a stator leakage reactance, which pertains to the flux that does not cross the air-gap, and the magnetizing reactance. In this per-unit system, the fictitious PM winding reactance, m_{mf}, and the magnetizing reactance on the d-axis, x_{md}, are defined to be equal. Note that since the PM windings are fictitious, one variable can be set, as long as the product of current and reactance is equal to the actual flux linkage. With this representation of the PM, the current from the source is constant, but the reactance is affected by the saturation in the circuit, and will be dependent on the currents.

$$
\begin{aligned}
\psi_d &= x_d i_d + x_{mf} i_f \\
\psi_d &= x_{s\sigma d}(i_d, i_q) \cdot i_d + x_{md}(i_d, i_q) \cdot (i_d + i_f)
\end{aligned}
\tag{35}
$$

$$
\begin{aligned}
x_d &= x_{s\sigma d} + x_{md} \\
x_{md} &= x_{mf}
\end{aligned}
$$

In this thesis, mainly the variation of stator current induced d-axis flux linkage will be analyzed, so the PM flux variation on this axis will be disregarded for some of the calculations. When the PM flux linkage is assumed to be constant, this leads to the ψ_m term being eliminated from the derivative of the d-axis flux linkage, as in the inductance definitions above. However, there will be done a discussion on this simplification and possible effects of it.

2.8 Goodness-of-fit statistics

In order to evaluate different models later on, some definitions are needed regarding the goodness-of-fit of curve fittings. The root mean square error (rmse) is a common statistical measure of deviation between actual values and predicted or modeled values, where naturally the error should be as close to zero as possible. The coefficient of determination, R^2 is also a standard measure of how well a model predicts the result, and lies between zero and one, where a value of one represents a perfect model fit. The adjusted coefficient (adj. R^2) has taken the degree of freedom in the models into account, so the statistic is not lower simply because of more independent variables. These are both displayed in equations 36 and 37, where f_i are estimated values, and y_i are observed values, with N being the number of observations and p is the number of independent variables in the model.

$$rmse = \sqrt{\sum_{n=1}^{N} \frac{(f_i - y_i)^2}{n}} \tag{36}$$

$$R^2 = 1 - \frac{\sum_{n=1}^{N}(f_i - y_i)^2}{\sum_{n=1}^{N}(y_i - \overline{y})^2}$$

$$adj.\ R^2 = 1 - \frac{(1 - R^2)(N - 1)}{N - p - 1} \tag{37}$$

3 IPMSM testing and results

There are many different procedures that can be used for identification of magnetic motor models, but in this thesis a constant-speed identification method was used [15]. In this method, the motor to be evaluated was connected with a speed-controlled motor thorough a common axle. By keeping a steady speed and varying the applied current the measured flux can be mapped to the applied stator currents in the motor.
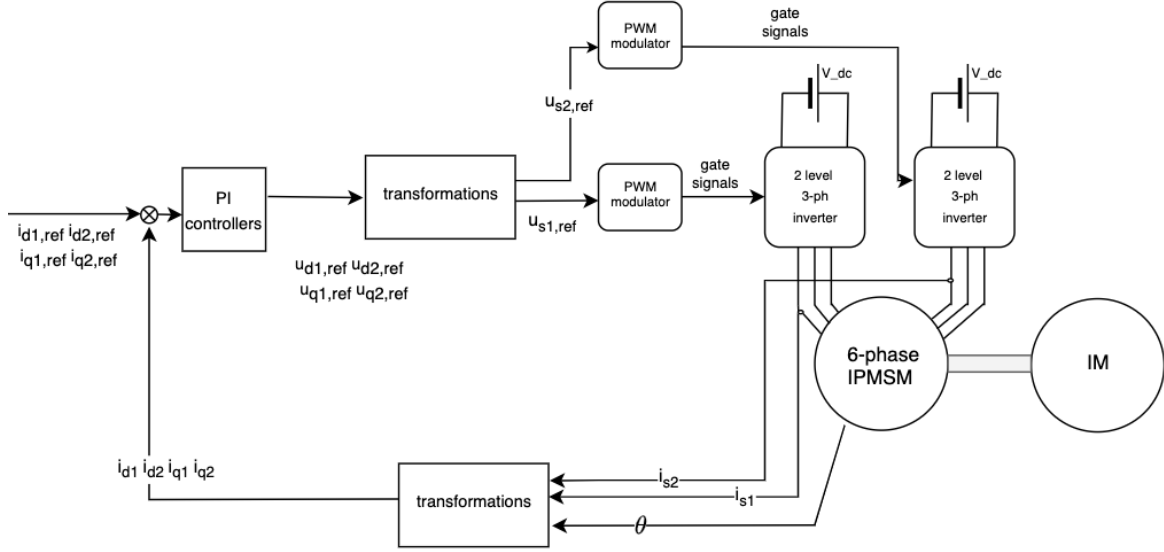
3.1 Experimental setup

Figure 9: General illustration of main components in motor lab setup

A SIEMENS 6-phase Permanent Magnet Synchronous Machine was used for the lab-tests. The 6 phase input currents was supplied by two separate PWM-controlled three-phase two-level inverters, each supplied with a voltage of 220V from a DC-source. There were inner current controllers of the PI type for both of the two winding sets. Four voltage references were supplied by the PI current controllers, and were transformed and forwarded to where the signals needed for PWM were calculated. The PWM modulators then controlled the two sets of inverters by supplying gate signals. The PI controllers took in the difference between measured signals from the stator current, and the manually set current references. The general workings of PI controllers is described by equation 38, where e is the difference between reference and measured value of the process variable, K_p represents the proportional gain, and T_i is the integration time constant. The time constants used in the lab control system are presented in equation 39, for both axes controllers.

$$u = K_p e + \frac{K_p}{T_i} \int e \ dt \tag{38}$$

$$T_d = \frac{x_d}{\omega_n r_s}$$
$$T_q = \frac{x_q}{\omega_n r_s} \tag{39}$$

The whole setup can be seen in figure 9. The transformation of currents and voltages between different reference frames was presented in chapter 2.3, using the measured six-phase currents and rotor angle from an encoder. Originally, the control system was more complex, with a cascade control structure, an inner current control loop and outer loops. The system could be run in a mode controlling the speed, or the torque, and the outer loops forward the references to the current controllers, based on the manually chosen outer loop references. In this setup however, it was desirable to control the d- and q- axis current references manually. Therefore, the functions determining current references from the outer torque or speed reference were removed in the code, effectively removing the outer loop.

16

Motor parameter	Value
N_n	2000 rpm
ω_n	628.32 rad/s
p	3
U_n	336 V
I_n	11.5 A
r_s	0.02 p.u.
ψ_m	0.954 p.u.
x_d	0.39 p.u.
x_q	0.985 p.u.
$x_{\sigma s}$	0.10 p.u.

Table 1: Motor data

The motor data can be seen in 1, where the d- and q- inductance values were measured at rated load [3]. The IPMSM's axle was connected to an Induction Motor (IM), which worked as a load for the PM Machine. The IM also had its own control system, inverters and voltage supply. The motors were controlled and observed using WatchView, running a Xilinx Software Development Kit (SDK)-code where the controllers were implemented and the measurement data from the motor was processed. Base-values for per-unit scaling were calculated, and transformations between reference systems were done in this code. This SDK-code was built at the Department of Electric Energy at NTNU, and slightly modified to the conducted experiments with help from supervisors at the department. Using this setup, the most relevant output signals from the motor or inverters could be read in real-time or as average values, in actual values or per unit, two-phase or three-phase etc.

3.2 Experimental procedure

The IPMSM evaluation was conducted with a constant input voltage of 220V DC, a constant speed reference of 0.1 p.u. and currents ranging from 0 to -1 p.u. for i_d and 0 to 0.8 p.u. for i_q. The initial step size for the currents were 0.2 p.u., but due to torque limitations in the Induction Motor a step size of 0.1 p.u. was used in the higher absolute values of i_d and i_q. In order to minimize the impact of temperature increase, which would affect the magnetic materials, the tests were done with as short elapsed time as possible.

In this setup, the speed of both motors was determined by controlling the IM in speed mode. Here, the torque on the two motors is balanced to obtain the reference speed, as follows from Newton's second law for rotation, see 40. A natural limitation to this setup was that the torque produced on the IPMSM would have to be within a range that the induction motor could match so as to keep the speed at its reference. In order to maximize the range of the testing currents, without excessive increase in input voltage, a low speed reference was chosen.

$$J\frac{d\Omega}{dt} = T_e - T_L \tag{40}$$

In the second quadrant, where negative i_d contributes to weakening the flux, a shorter step size and data-point omission was used to keep the electric torque within the limit of the Induction Motor. This was performed at i_d values of -0.6 p.u. and below. Specifically at i_d values of -0.6, -0.8 and -1.0 the highest i_q values were 0.7, 0.6 and 0.6 respectively. In addition an extra evaluation point at i_d -0.7 p.u. and i_q 0.7 p.u. was included in order to obtain a more complete mapping. These evaluation points can be seen in figure 11 and 10 in chapter 3.3 later on.

$$m = \frac{U_0}{U_{dc}} \tag{41}$$

In addition, the PWM modulation-index was monitored during testing, as it would indicate if the inverts went into overmodulation. Equation 41 is the relation between a PWM modulation index, output voltage and the input dc-voltage, where a modulation index above unity is overmodulation. The voltage waveform from the inverters can become distorted with lots of harmonics when the output magnitude is increased too much, i.e. if one goes too far into overmodulation. In order to avoid this, a maximum modulation index of 1.15 was used in the setup. The currents could only be increased so much before the voltage would cause the modulation index to surpass this level, which naturally became a limitation in the setup.

3.2.1 Data processing

The base-value calculations in the SDK-code ensured that it was possible to read all results in p.u.values, and unless stated otherwise, all results are given in p.u. throughout the thesis. While conducting the tests, the speed, d- and q-axis currents and d- and q-axis voltages were registered from WatchWiew. Using the voltage and current measurements from the tests, the d- and q-axis flux linkages were calculated using equation 42, which is derived from equation 18 and 19 presented in chapter 2.4, but where the system is in steady state and the flux derivative term in the original motor model therefore is zero.

$$\psi_d = \frac{u_q - r_s i_q}{n}$$
$$\psi_q = \frac{-u_d + r_s i_d}{n} \tag{42}$$

The measured d- and q-axis flux values at 0.01 q-axis current were evaluated, and were found to correspond to a rotor angle of 0.66 deg. This was close to the estimated sample delay angle error of 0.75 deg, computed using equation 43. For all flux values, this error was calculated based on the measured speed, and the d- and q-axis flux linkages without this angle shift were computed. The q-axis flux at zero current was closer to zero after adjusting for the angle error. It should be noted that the angle error was found to be small, and the effect of this error adjustment on the data was negligible.

$$\theta_{samp} = \frac{d\theta}{dt} 1.5 T_{samp} = \omega_n n 1.5 T_{samp} \tag{43}$$

The tests were conducted for several quadrants, but as mentioned previously more datapoints were tested in the second quadrant. The reason why the second quadrant was chosen is that it is with negative d-axis and positive q-axis currents that the electric torque is both positive and at its highest, which can easily be seen by plotting the torque equation 22 with current vector angle as the varying parameter, seen in figure 5. This is generally the only quadrant that is used when the IPMSM is run in real life, so it was decided to focus more on this quadrant in the further analysis.

3.3 Curve fitting method

Curve fitting different dataset to model functions is an essential procedure in this thesis. The curve fitting was generally done with two different methods. The fit function from MATLABs Curve Fitting Toolbox, which fits a dataset to a specified model function, was used. The function finds an extrapolation algorithm suited for the applied model. The trust-region-reflective algorithm was automatically assigned to the curve fits in this thesis.

However, it was not possible to fit two separate datasets to two different model functions with common coefficients using the MATLAB Curve Fitting Toolbox fit function, and therefore another method was needed. Fitting two dataset to two models with common coefficients was desired in several of the models where the reciprocal condition was being enforced. In order to do this, the multiple linear regression function in MATLAB was used, setting $\boldsymbol{Y}$ to the data of the parameter to be fitted, and defining vectors of the different polynomial terms of the state variables, which go into the $\boldsymbol{X}$-matrix. The resulting $\boldsymbol{b}$-vector then contains the approximated model coefficients, following the standard linear regression equation in 44.

$$\boldsymbol{y} = \boldsymbol{Xb} \tag{44}$$

When the results of a fitting was done, in addition to the curve fit coefficients, the goodness-of-fit statistics were given, making it possible to evaluate the curve fit underway and ensure that the fit was satisfactory. Mostly, the root mean square error and adjusted coefficient of determination were monitored, which were presented in chapter 2.8. These two statistics are easily accessible both in MATLAB and by straightforward calculations, and are useful tools for evaluating the results during the curve-fitting process, giving statistical indication of the quality of the fit in addition to the observable visual fit. Other statistics could have been chosen as well, but regardless of the choice, consistency in the choice across the evaluation of all fits was deemed most important for a meaningfully comparison.

3.4   Motor test results

The resulting d- and q-axis flux linkage plots from the testing and processing explained in chapter 3.2 are shown in figures 10 and 11. Here, the datapoints are connected in a simple surface plot. The IM was run at a reference speed of 0.1, giving a speed of 0.11 p.u. on the IPMSM.
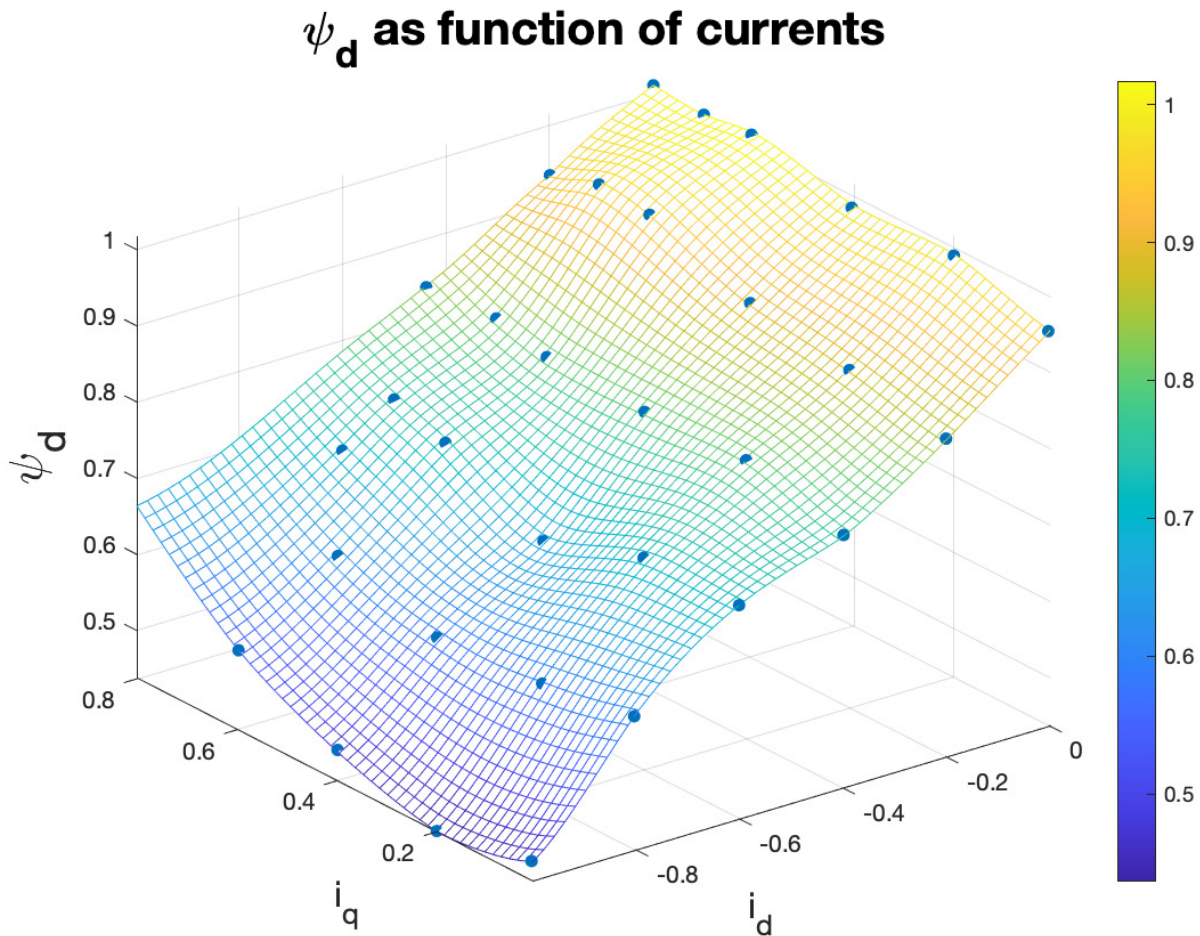

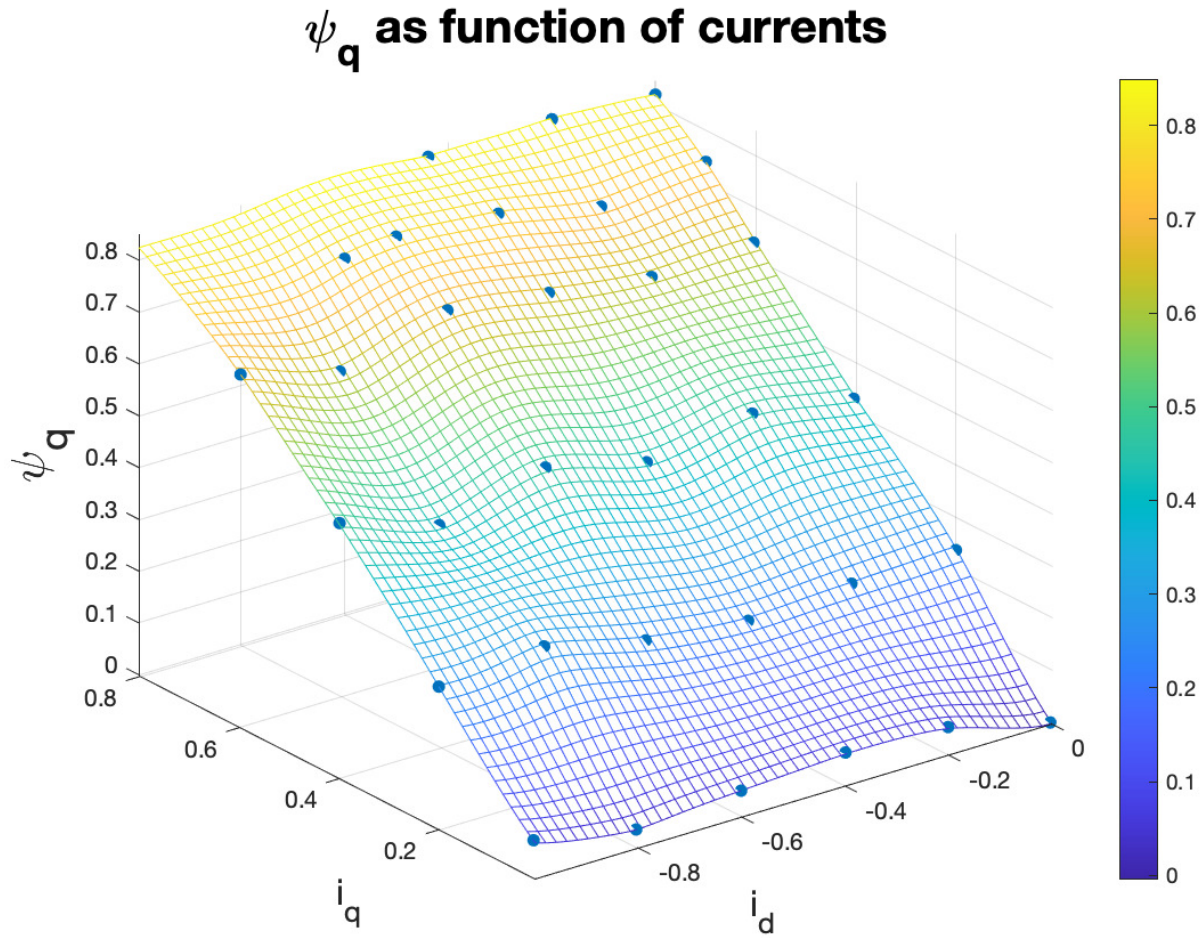Figure 10: Measured flux linkage on d-axis at 0.11 p.u. speed

Figure 11: Measured flux linkage on q-axis at 0.11 p.u. speed

3.4.1 No-load datapoints

Firstly, in order to ensure that the data is realistic, the datapoints at zero current are important and should be analyzed. The datapoints at approximately zero current, or no-load, is displayed in table 2. The flux linkage plot where the two currents each are approximately zero are shown in figure 12. These plots are essentially cross-sections of the 3D-plots in figures 10 and 11. By observing the flux when one of the currents is zero, one can see the self-inductances more clearly, as is understood through the definition of self- and cross-coupling inductances in equation 32. A simple linear curve fit was also done and plotted together with the datapoints in the same figure in 12.

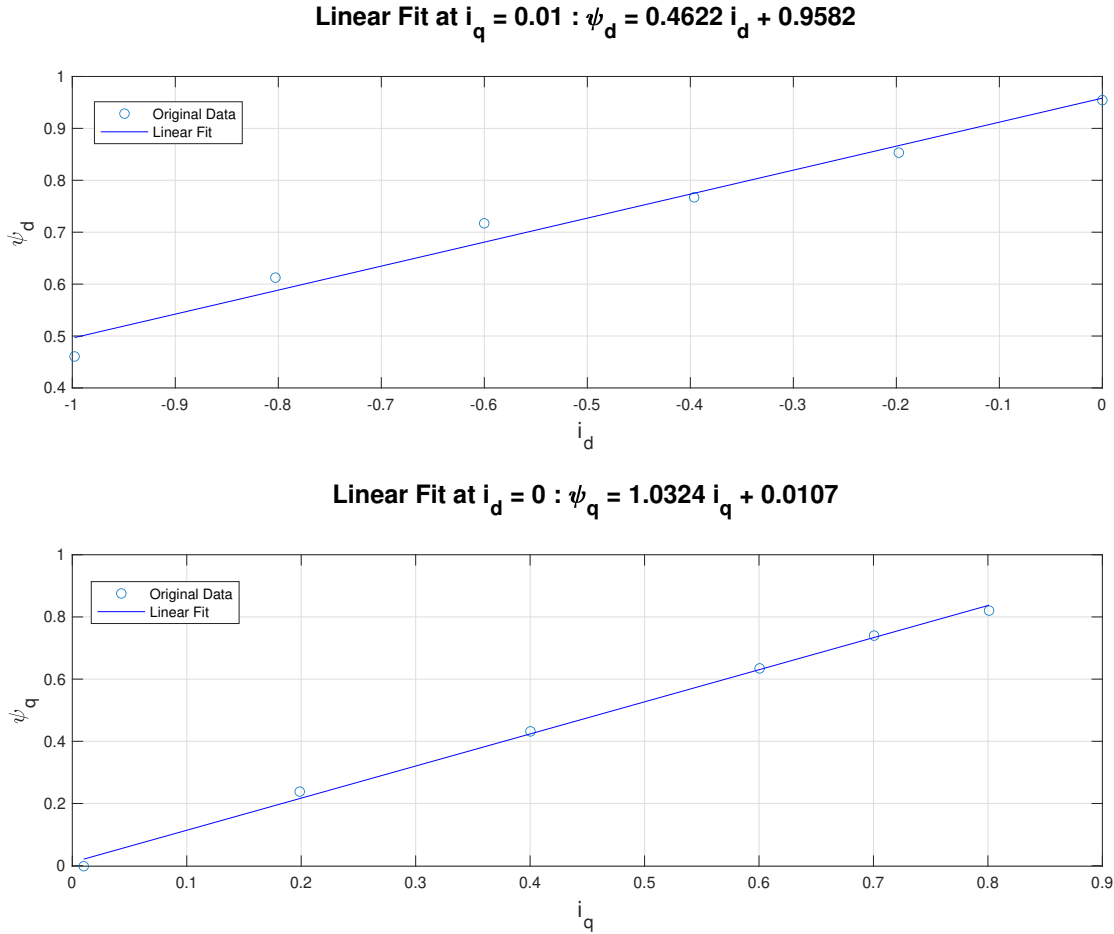| n	i_d	i_q	ψ_d	ψ_q
0.1128	0.0000	0.0100	0.9544	-0.0017

Table 2: Measured data at no-load

Figure 12: Flux linkages and simple linear curve fit at 0.11 p.u. speed

It is visible here that when both currents are zero, the d-axis flux is very close to the previously known nameplate value for the PM flux, ψ_m, which is 0.954 p.u., and the q-axis flux is almost zero. This is in accordance with the general motor model equations presented in the theory. There should ideally be no flux linkage at zero current, apart from the flux set up by the PM. However, there is a small q-axis current in this test, allowing also for a small deviation from zero in the q-axis flux linkage. Next, from the cross-section plots and the linear fit coefficients in 12, the d- and q-axis linear rates of increase, which should be quite close to the two axis inductance values x_d and x_q, are around 0.46 and 1.03 respectively. These values look reasonable compared with previously given data seen in table 1, where the d- and q- axis inductances L_d and L_q is 0.39 and 0.99 respectively. Since only a simple linear fit for the two cross-sections were conducted, a perfect match between the respective values were not expected. Still, the values were evaluated to fall within reasonable and expected limits.

3.4.2 Self-inductances, cross-coupling and saturation

In order to examine the inductances, cross-coupling, and possible saturation, several more cross-section data are plotted in figure 13. Here, one current is the independent variable while the other current is a parameter. In this way, the differential self- and cross-coupling inductances are visible. There were also done calculations of the differential inductances according to equation 33. However, the steps between the lab data currents were quite large, resulting in plots with pronounced deviations and unevenness. Consequently, deriving any meaningful analysis from it was not possible.
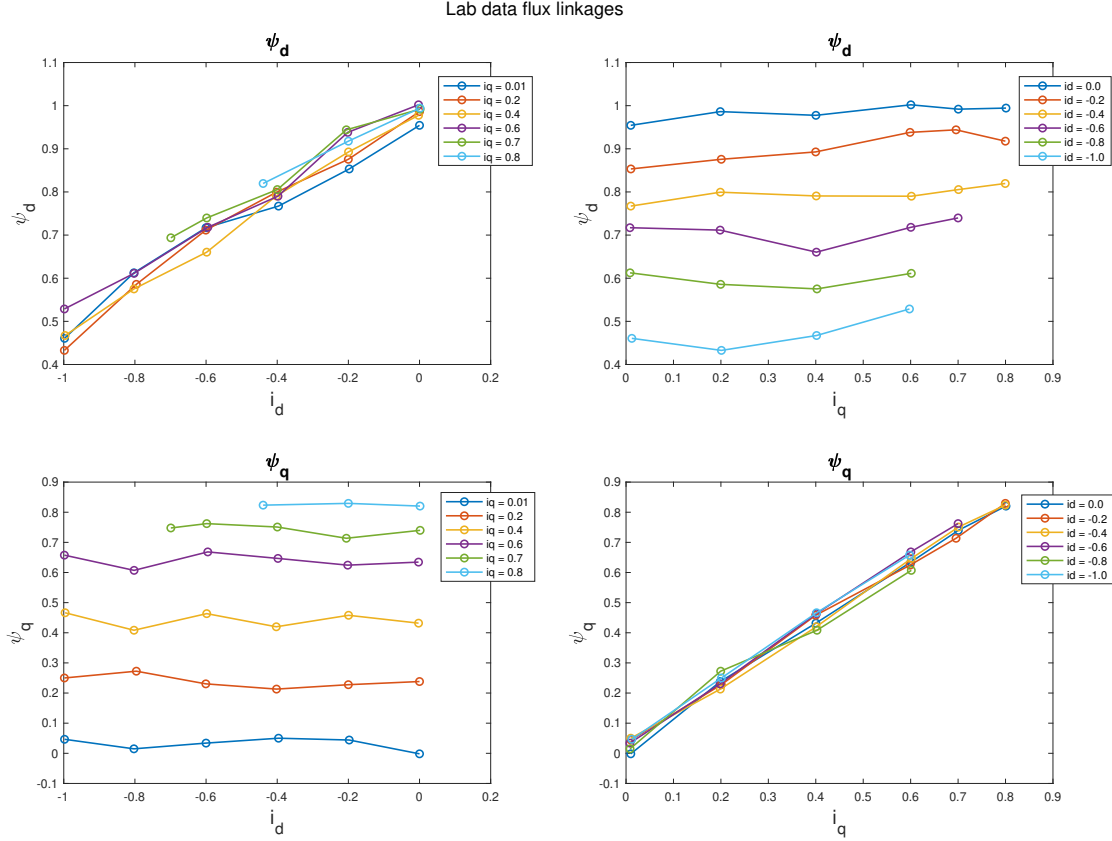
Figure 13: Lab data: flux linkages on d- and q-axis plotted against d- and q-axis currents

From figure 10 presented previously, the d-axis flux linkage is clearly dependent on both currents, meaning there is some cross-coupling visible. It is also notable that there are few points that distort the smooth plane shape to a certain degree. The dependence on the d-axis current is large, as expected, but there is no clear trend that the rate of increase is higher for certain i_d values in figure 13, where the d-axis flux is plotted against the d-axis current. It is reasonable to gather that the self-inductance does not vary much for different i_q in this test range, though some datapoints deviate a little from the trends. Similarly to at the zero-current datapoint, the rate of increase is around 0.5, which is not too far from the expected inductance value. Next, the d-axis flux increases with increasing i_q, but the dependence on i_q is varying somewhat at different d-axis currents, as can also be seen in figure 13. It is quite difficult to determine a trend from this variation, but one could note that the cross-coupling inductance drops a little for higher d-axis currents at higher q-axis currents.

In figure 11 of the measured q-axis flux, which was presented previously, it is possible to observe that also on this axis there is some cross-coupling-effect, and that there is a high self-inductance. Figure 13 shows that the rate of increase of the q-axis flux when increasing i_q is more or less constant and equal regardless of i_d value. In other words, also on this axis the self-inductance seems to be constant, and at 1.0 p.u., the value is reasonable. Lastly, q-axis flux dependence on i_d, seen in the same cross-section plots, is quite small. One can note that the flux increases with more negative d-axis current, for all q-axis currents, and apart from this there is no clear pattern. In total, the results show some cross-coupling, but it is small on both axes. When studying the plots closely, it can seem like the d-axis flux sees a little more cross-coupling than the q-axis flux. For both fluxes, the self-inductance is very much dominant. In addition, the self-inductance seems almost constant, while there is quite a bit of disturbance on the d-axis self-inductance, regardless of the q-axis current i_q. One reason can be that the PM flux varies, or that there is some saturation.

There is no or very little saturation visible in the results. As noted, it is possible to observe a little bit of a fall in the d-axis flux at high q-axis currents and d-axis currents close to zero. Since the negative d-axis currents will decrease the total flux and move the motor to less saturation on the d-axis, and high q-axis currents likely saturate the d-axis, this is the area of the second quadrant where it is most likely to appear visible d-axis saturation effects. Still, there are too much deviation in the plots to know if this is saturation for sure or simply deviation or errors measurement or data processing. In any case, there are no obvious saturation phenomena.

3.5 Curve fittings of flux linkages and currents

The flux linkage data from the conducted tests were next fitted to the polynomial functions in equations 45 and 46, with currents and flux linkages as state variables, respectively. The first model in equation 45 was developed in the master thesis of Sommer Klyve (2021) [2]. The model is designed such that it is possible to fulfill the reciprocal condition. It was also further explored in the master thesis of Hoseny Uosef (2023) [16], where the second model, equation 46, was deduced through curve fitting and simplification.

$$\psi_{dm} = d_{10}i_d + d_{11}i_d i_q + d_{02}i_q^2 + \frac{1}{3}q_{12}i_q^3$$
$$\psi_q = q_{01}i_q + q_{02}i_q^2 + q_{12}i_d i_q^2 + \frac{1}{2}d_{11}i_d^2 + 2d_{02}i_d i_q \tag{45}$$

$$i_d = d_{10}\psi_{dm} + d_{13}\psi_{dm}\psi_q^3$$
$$i_q = q_{01}\psi_q + q_{03}\psi_q^3 + q_{22}\psi_{dm}^2\psi_q^2 \tag{46}$$

The curve fit plots with current as state parameter are shown in figure 14 on the next page. A plot of the curve fit with flux linkage as state variable was also run, resulting in a worse visual fit, and this plot has not been included. The coefficients from both the curve fits are presented in tables 3 and 4. As seen in the tables, a few of the coefficients have high uncertainty within a 95 % confidence interval, especially in the models with flux as s.v., where the number of terms are also smaller.

Coefficient	Value
d_{10}	2.127
d_{13}	0.795*
q_{01}	0.810
q_{03}	0.203*
q_{22}	1.193*
$1/d_{10}$	0.470
$1/q_{01}$	1.235
rmse	0.059
adj.R^2	0.986

Table 3: Coefficients from curve fit of lab data to model 46, flux as state variable
*This value has a very large confidence bounds

Coefficient	Value
d_{10}	0.445
d_{11}	0.089
d_{02}	0.249
q_{01}	1.355
q_{02}	-0.412
q_{12}	-0.622*
rmse	0.0254
adj.R^2	0.995

Table 4: Coefficients from curve fit of lab data to 45, current as state variable
*This value has a very large confidence bounds

Curve Fit: $\psi_{dm} = 0.45\, i_d + 0.09\, i_d\, i_q\, 0.25\, i_q^2 + \text{-}0.62\, i_q^3/3$

$i_q = 0.00$

$i_q = 0.20$

$i_q = 0.60$

$i_q = 0.70$
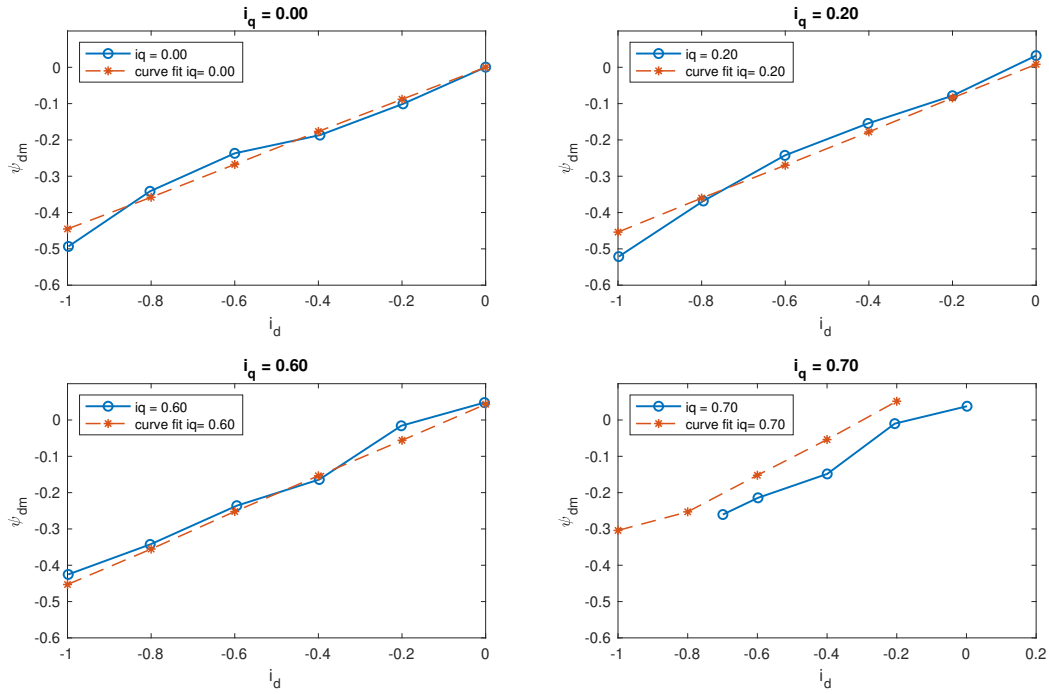
(a) Stator current induced flux linkage on d-axis

Curve Fit: $\psi_q = 1.36\, i_q + \text{-}0.41\, i_q^2 + \text{-}0.62\, i_d\, i_q^2 + 0.09\, 0.5\, i_d^2 + 0.248\, 2\, i_d\, i_q$

$i_d = 0.00$

$i_d = \text{-}0.20$

$i_d = \text{-}0.60$

$i_d = \text{-}1.00$
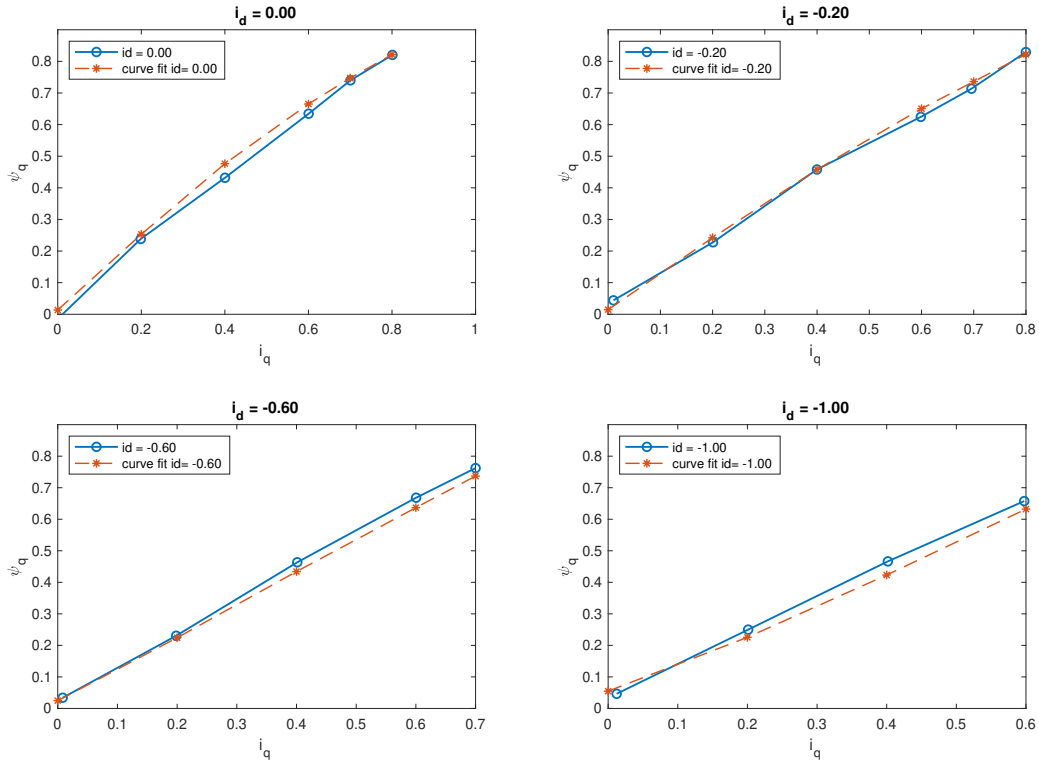
(b) Flux linkage on q-axis

Figure 14: Curve fit of model 45 to lab results

24

In both these curve fittings, the reciprocal condition is fulfilled, as can also be seen by calculating the two self-inductance expressions of the curve-fit functions and observing that equation 34 is valid. For current as state variable, the condition is fulfilled when the common coefficients are the same for both equations in 45, as seen in equation 47. For flux as state variable, equation 48 has to be fulfilled, as can easily be seen through partial derivation. The curve-fits were also run where the reciprocal condition not being enforced. The results from this can be found in the appendix, in tables 14, 15, 12 and 13. The curve fit was a perhaps a little better without the reciprocal condition being enforced, but the difference is small. Lastly, the self- and cross-coupling inductances based on the lab curve fit to 45 is found in the appendix.

$$\frac{\partial \psi_{dm}}{\partial i_q} = d_{11}i_d + 2d_{02}i_q + q_{12}i_q^2 = \frac{\partial \psi_q}{\partial i_d} \tag{47}$$

$$\frac{\partial i_d}{\partial \psi_q} = 3d_{13}\psi_{dm}\psi_q^2 = 2q_{22}\psi_{dm}\psi_q^2 = \frac{\partial i_q}{\partial \psi_d} \tag{48}$$

$$3d_{13} = 2q_{22}$$

3.5.1 What to take from the curve fittings

The curve fit plots in figure 14 illustrate that the model functions in equations 45 and 46 model the measured data quite well. However, it is clear that these functions are not able to capture all the variation that exists within the data. Especially on the d-axis stator induced flux linkage in 14a, which is fitted to the third-degree four-term polynomial, there is a bit of deviation from the curve. The q-axis flux is visually a better fit, but it should be noted that this model has more terms than the d-axis model. As previously noted, there are some datapoints that deviate from the expected values, and one should acknowledge that it is not possible for third and fourth-degree polynomials with limited number of terms to include all variations in the dataset. For this, one would likely need larger or higher degree functions. However, the most important aim here is not for the model to fit to all deviating datapoints, but rather to capture the trends in the data as good as possible.

Next, high intervals of confidence indicate that the model coefficients would change considerably if there are even small changes in the data. Still, these particular coefficients relate to higher-degree terms, which make up relatively smaller parts of the output currents or flux compared to the first-degree terms. Especially in the test range that is used, where the current and absolute flux values are well below zero, these terms are small.

The two coefficients d_{10} and q_{01}, which were also presented in table 4, are the constant terms of the self-inductance expressions. These should be reasonably close to the inductances that were found previously in the linear fit at zero current, since the curve fit should be consistent with the plotted results. The same is the case for the inverse of d_{10} and q_{01} in table 3, as these two coefficents very much impact the self-inductances. The values of $1/q_{01}$ and q_{01}, relating to the self-inductance on the q-axis, are quite a bit different from the linear values, indicating that there is in fact not the linear terms that dominate, but that the higher-degree terms relating to cross-coupling and saturation are significant as well.

Next, it is notable that the curve fit seems to be slightly better when there is no restraint on the coefficients from the reciprocal condition. This leads to a proposition that the motor results perhaps do not completely fulfill the reciprocal condition. It is a possibility that the value of stator resistive losses that is used when calculating the fluxes in 42 is not precise or varies. In that case, the calculated relation between the d-axis current and q-axis flux, and the q-axis current and d-axis flux, would differ slightly from the real motor values. There is also a risk of measurement errors in the lab-setup. There were small oscillations on the output signals during the test, also in steady-state, meaning that each datapoint in the plot was in reality a random point in a very small radius around the precise reference value. In other words, there was likely to be small precision errors on some datapoints when the instantaneous values were taken. Some tests were rerun where there was a suspicion that the measured datapoint was too far from the average value. Another possible explanation could be that the curve fit is not perfect, meaning that the condition could be fulfilled in the data, only that the curve fit is not precise enough.

4 Stumberger et al. Study of Saturation and Cross-Magnetization in IPMSM

In order to compare the results from the lab tests and further analyze the motor cross-coupling and saturation, a study based on previous published motor tests was conducted. The work in the subsequent section was based on the work and data from Stumberger et al. (2003) [6], in which a thorough investigation of flux linkage and current relations in an IPMSM was performed. In this paper, there was run locked rotor tests while controlling current and voltage components, with aim to observe saturation and cross-coupling phenomena. The motor that was tested had two pole-pairs and 24 slots, the PMs aligned in tangential configuration, and rated power and current was 0.676kW and 1.49A, respectively. The motor was supplied by a controlled voltage source inverter.

$$\psi_d = \int_0^t u_d(\tau) - r \cdot i_d(\tau) \, d\tau \tag{49}$$

In the tests, one of the two axes currents was kept constant, while the other axis current varied while a stepwise voltage form was applied on that same axis. The varying current was measured and the resistance was calculated for each voltage step. The flux linkages was calculated using equations18 and 19, previously presented in the theory section. The locked rotor position, i.e. zero speed, eliminates the back-emf term of the voltage equation. From this, the integral of the stepwise voltage and the resistive voltage drop was calculated, as seen in 49, and the results were a very precise mapping of flux linkage and current. When this was done for a range of different constant currents as well, we get a 3 dimensional mapping of d- and q-axis flux to the two axes currents. Note that any constant value present in the flux linkages is naturally not captured in this integral-method.

$$L_{dd} = \frac{\partial \psi_d}{i_d} \approx \frac{\Delta \psi_d}{\Delta i_d}\bigg|_{i_q=c} \qquad\qquad L_{qd} = \frac{\partial \psi_q}{i_d} \approx \frac{\Delta \psi_q}{\Delta i_d}\bigg|_{i_q=c}$$

$$L_{dq} = \frac{\partial \psi_d}{i_q} \approx \frac{\Delta \psi_d}{\Delta i_q}\bigg|_{i_d=c} \qquad\qquad L_{qq} = \frac{\partial \psi_q}{i_q} \approx \frac{\Delta \psi_q}{\Delta i_q}\bigg|_{i_d=c} \tag{33}$$

The self- and cross-coupling inductances corresponded to the partial derivatives of the flux linkages, as presented previously, and could also be approximated by the partial differences in the data, shown in 33. In order to find partial derivatives over the whole range of flux linkages, these data were approximated by continuous exponential functions. The partial derivatives were plotted in the paper, along with the flux measurements and 2D FE flux-current calculations where saturation was taken into account through a hysteresis curve.

4.1 Data extraction

A plot digitization software was used to extract the datapoints from the plots of the flux linkages and self- and cross-coupling inductances in the paper. The data was then exported to MATLAB, for further analysis. Several curve fittings were done. Firstly, the flux linkages were approximated by a set of model functions. Next, the inductances were approximated through curve fitting, and flux linkage models were developed from this. The raw digitized data from the Stumberger study are presented in figures 15a and 15b.
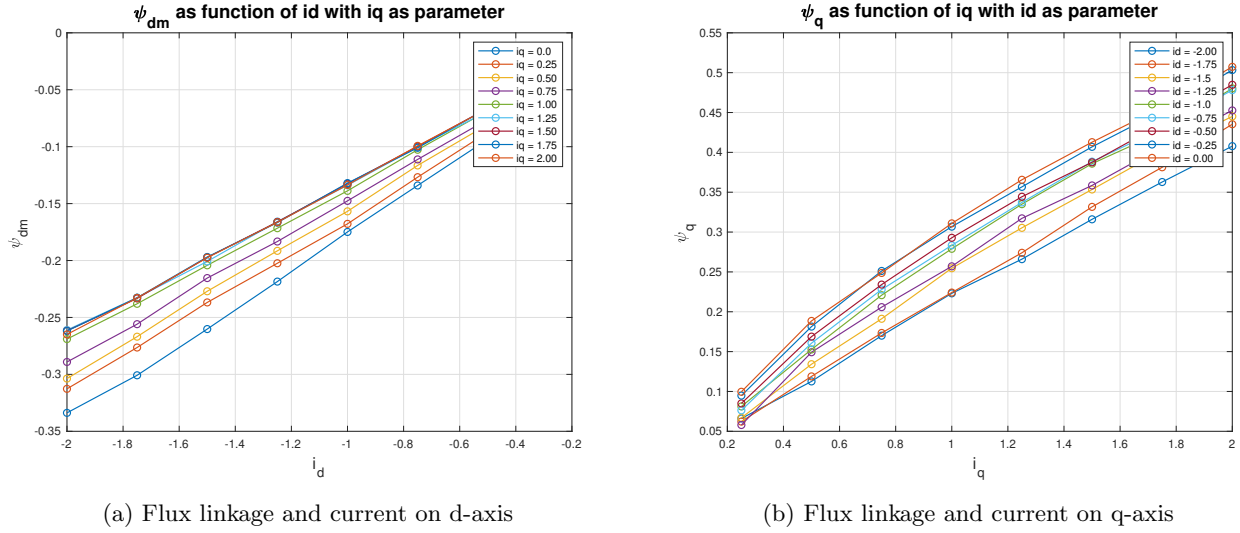
(a) Flux linkage and current on d-axis   (b) Flux linkage and current on q-axis

Figure 15: Raw data extracted from Stumberger et al.

4.2 Curve fitting

In order to describe the phenomena and tendencies in the flux linkages, this data was curve fitted to several functions. The two functions that are shown in equations 50 and 51 were chosen based on visual analysis of the flux linkage dependences on the axis currents. Currents were chosen as state variables when developing models from this point and onward, because it makes the most sense in terms of evaluating the magnetic saturation. The resulting fit to the data was very good. In addition the calculated root mean square error when curve fitting these functions to the data was quite small and the number of higher degree terms is limited.

$$\psi_{dm} = \left(d_{10} - d_{11}|i_q| + d_{12}i_q^2 \right) i_d \tag{50}$$

$$\psi_q = \left(q_{01} + q_{11}i_d - q_{02}|i_q| \right) i_q \tag{51}$$

Coefficient	Value
d_{10}	0.172
d_{11}	0.049
d_{12}	0.015
rmse	0.0036
q_{01}	0.343
q_{11}	0.032
q_{02}	0.040
rmse	0.012

Table 5: Coefficients from curve fit

The coefficients are presented in table 5, and the curve fits and data points are shown in figures 16 and 17. Full 3D figures of the curve fits with data points were also done to ensure that the fit was satisfactory for the entire range of datapoints. Note that the integration method used to calculate the fluxes did in fact only calculate the variation in flux and not the constant terms, meaning that the PM-induced flux on the d-axis is excluded in both the plots and the curve-fit function.
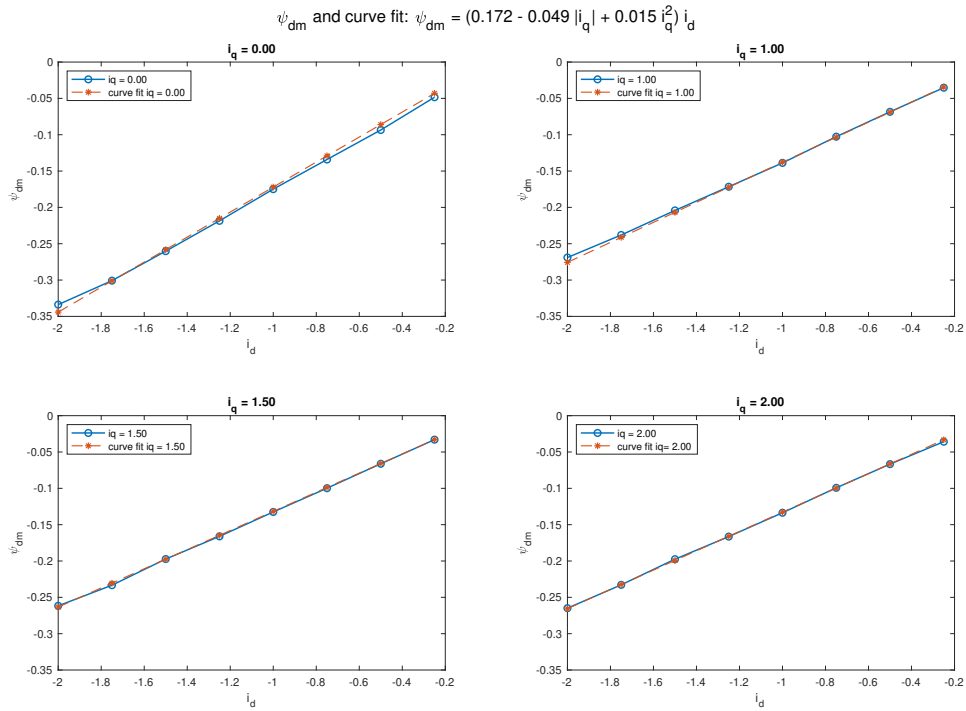
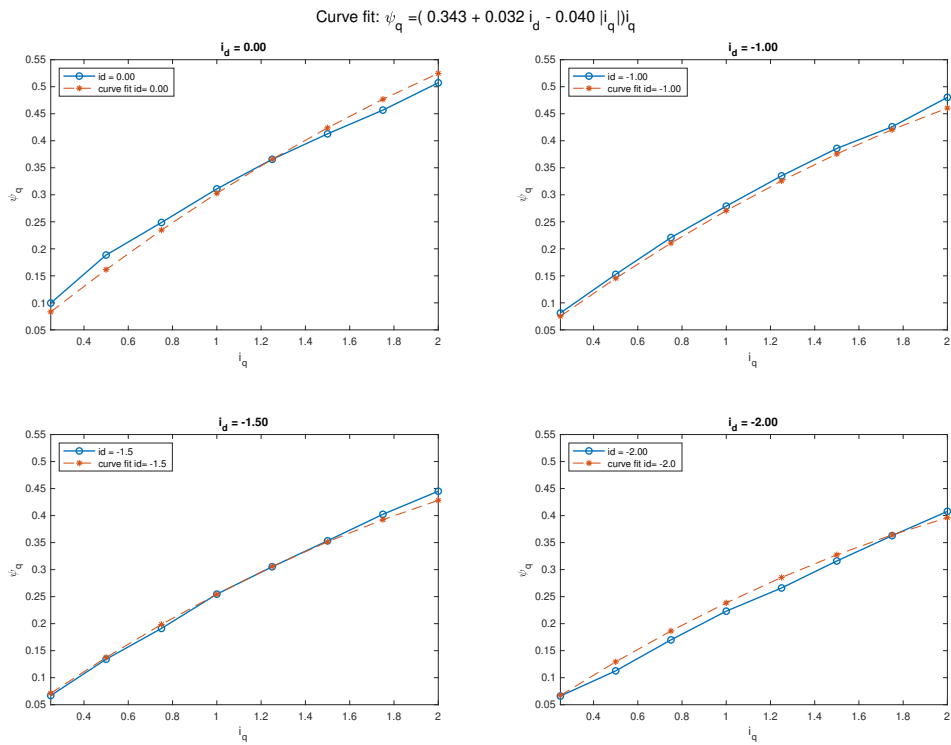Figure 16: Curve fit to d-axis flux linkage variation

Figure 17: Curve fit to q-axis flux linkage variation

Both curve fit models are expressed as a self-inductance function times the same axis current, as seen in the equations 50 and 51. In both these flux linkage functions, there is a term only dependent on the same axis current, or a constant term in the inductance expression. In the d-axis function, there is one term decreasing with the absolute value of the q-axis current, and one term increasing with the square of it. The d-axis self-inductance is not dependent on the d-axis current in the curve fit, which is consistent with the observations done from the plots above. Next, the q-axis flux has one term that increases with the d-axis current and one term that decreases with the signed square of the q-axis current.

$$\frac{\partial \psi_{dm}}{\partial i_q} = -0.049 i_d + 2 \cdot 0.015 i_q i_d$$

$$\frac{\partial \psi_q}{\partial i_d} = 0.032 i_q$$

(52)

The reciprocal condition, which has been introduced in the theory, is clearly not fulfilled for the data, which is seen by again observing the partial derivatives of the curve fit in equation 52. When the two partial derivative curves are plotted, it is visible that they differ in shape, but that the magnitudes are close to equal.

4.3 Development of new flux models

In order to understand the cross-coupling and saturation phenomena more thoroughly, it was necessary to create models that capture as many trends as possible in the flux linkage to current mapping. These will necessarily be more detailed and include trends seen in the differential inductance plots.

$$\psi_{dm} = \int L_{dd} \partial i_d + \psi_d(i_q) = \int L_{dq} \partial i_q + \psi_d(i_d)$$

$$\psi_q = \int L_{qd} \partial i_d + \psi_q(i_q) = \int L_{qq} \partial i_q + \psi_q(i_d)$$

$$L_{dd} = d_{10} - d_{11} i_q + d_{12} i_q^2 + 2 d_{20} i_d + d_{13} i_q^3 \tag{53}$$

$$L_{dq} = -d_{11} i_d + 2 d_{12} i_d i_q + 3 d_{13} i_d i_q^2 \tag{54}$$

$$\psi_{dm} = \left(d_{10} - d_{11} i_q + d_{12} i_q^2 + d_{20} i_d + d_{13} i_q^3 \right) i_d \tag{55}$$

$$L_{qd} = q_{11} i_q + 2 q_{21} i_d i_q + q_{12} i_q^2 + 3 q_{31} i_d^2 i_q \tag{56}$$

$$L_{qq} = q_{01} + q_{11} i_d + q_{21} i_d^2 + 2 q_{12} i_d i_q + 2 q_{02} i_q + 3 q_{03} i_q^2 + q_{31} i_d^3 \tag{57}$$

$$\psi_q = \left(q_{01} + q_{11} i_d + q_{21} i_d^2 + q_{12} i_d i_q + q_{02} i_q + q_{03} i_q^2 + q_{31} i_d^3 \right) i_q \tag{58}$$

The four differential inductance functions, 53,54, 56 and 57, were developed to fit the digitized values of the differential inductances from the Stumberger paper. Several methods were attempted to find the best functions. Lastly, a combination of visual analysis, MATLAB calculations of goodness-of-fit statistics and trial-and error was used. It was also a goal to find a polynomial that was detailed enough, while at the same time not making it too large with many insignificant high-degree terms. The differential inductances models were created such that the integral of two and two resulted in a common flux linkage model function. The general partial derivatives or inductances was presented in equation 32 in the theory chapter. By using the differential inductances as the basis of the models, the more detailed trends in the differential inductances are captured.

In total, the following demands were taken into consideration when defining the model functions:

- Good fit to data and trends for each differential inductance

- Compatible differential inductance functions for common integral

- Satisfactory fit of flux linkage function/integral to data

- Not overly large polynomials

The resulting model functions can be seen in equations 55 and 58. On the d-axis, the three terms pertaining to coefficients d_{11}, d_{12} and d_{13} all models the cross-coupling, while the terms related to d_{11} and d_{20} model the saturation, naturally dependent on the coefficient value. Next, on the q-axis, the q_{11}, q_{21}, q_{12} and q_{31} models cross-coupling, while mainly q_{02} and q_{03} provide saturation.

It can be noted that all terms in the d-axis flux linkage depend on the d-axis current, meaning that the flux linkage can be written as a d-axis inductance expression times the d-axis current, and the same is true for the q-axis. Even though there are several cross-coupling terms in the models, all depend on the same axis current.
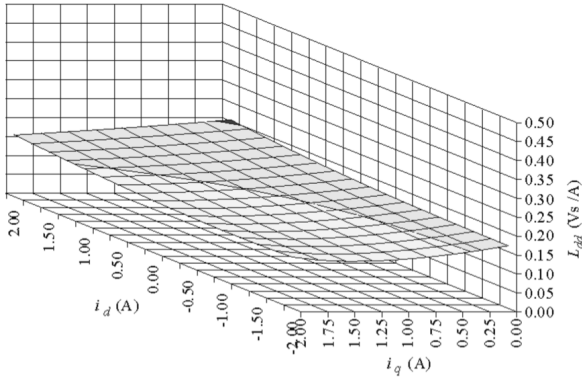
The differential inductances from the Stumberger paper and the curve fit based on the same data can be seen in figures 18, 19, 20 and 21. The coefficients of the curve fit is presented in tables 6 and 7. This was the curve fit where the differential inductances were fitted, and the flux models were based on these coefficients. There was also done curve fits of the digitized paper values of the flux linkages to the corresponding d- and q- flux model functions. The coefficients from this can be seen in 8 and 9, while the flux linkage plots are included in figures 22 and 23.

Coefficient	Value
d_{10}	0.174
d_{11}	0.041
d_{12}	0.007
d_{20}	0.003
d_{13}	0.002
rmse	0.002
adj.R^2	0.999

Table 6: Coefficients: Curve fit of Paper data inductances to model 53-57

Coefficient	value
q_{01}	0.329
q_{11}	0.038
q_{21}	-0.006
q_{12}	-0.011
q_{02}	-0.042
q_{03}	0.002
q_{31}	-0.001
rmse	0.001
adj.R^2	1.000

Table 7: Coefficients: Curve fit of Paper data inductances to model 53-57

(a) Figure from Stumberger paper
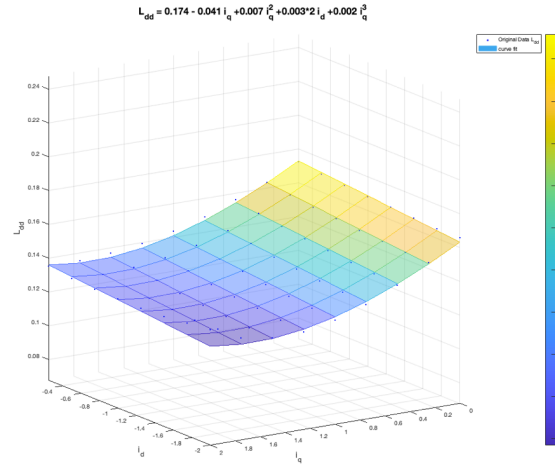
(b) Stumberger paper data curve fitted to model in 53

Figure 18: Differential inductance L_{dd}

(a) Figure from Stumberger paper

(b) Stumberger paper data curve fitted to model in 54

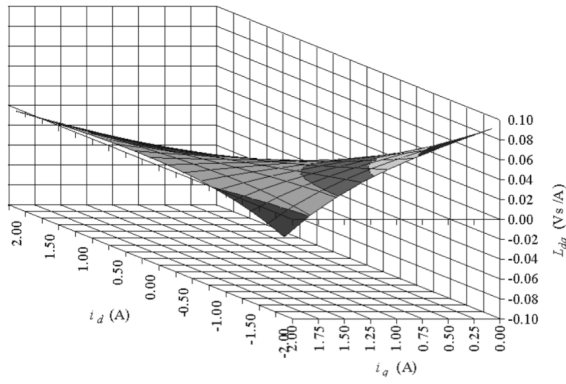Figure 19: Differential inductance L_{dq}
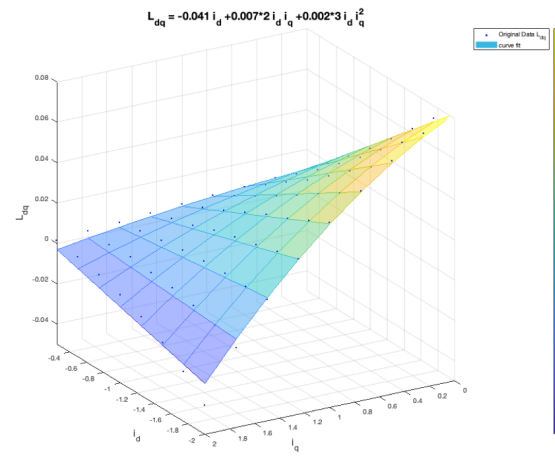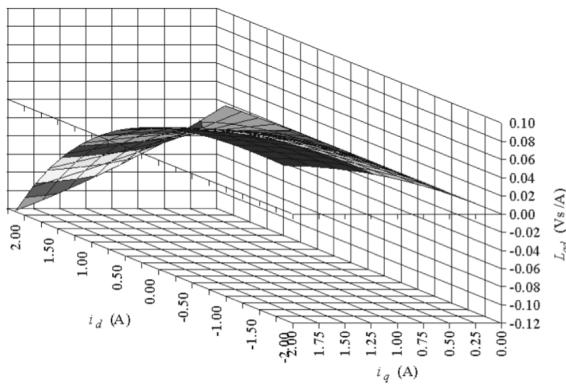

(a) Figure from Stumberger paper

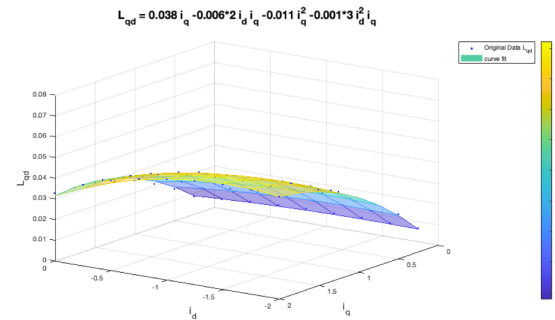(b) Stumberger paper data curve fitted to model in 56

Figure 20: Differential inductance L_{qd}

(a) Figure from Stumberger paper

(b) Stumberger paper data curve fitted to model in 57
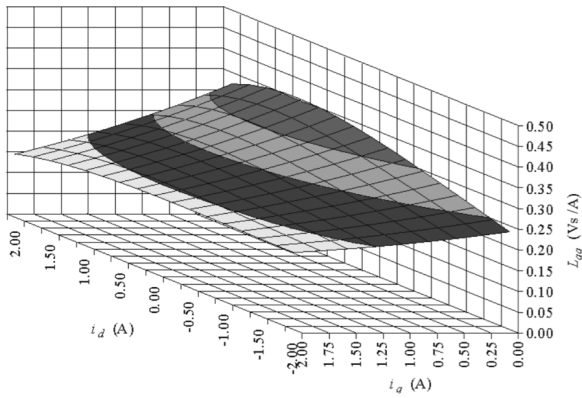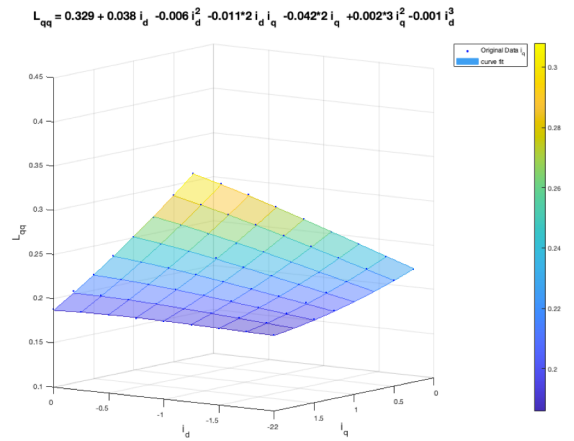
Figure 21: Differential inductance L_{qq}

Curve Fit: $\psi_{dm} = 0.178\, i_d + 0.045\, i_d\, i_q + 0.009\, i_d\, i_q^2 + 0.004\, i_d^2 + 0.002\, i_d\, i_q^3$
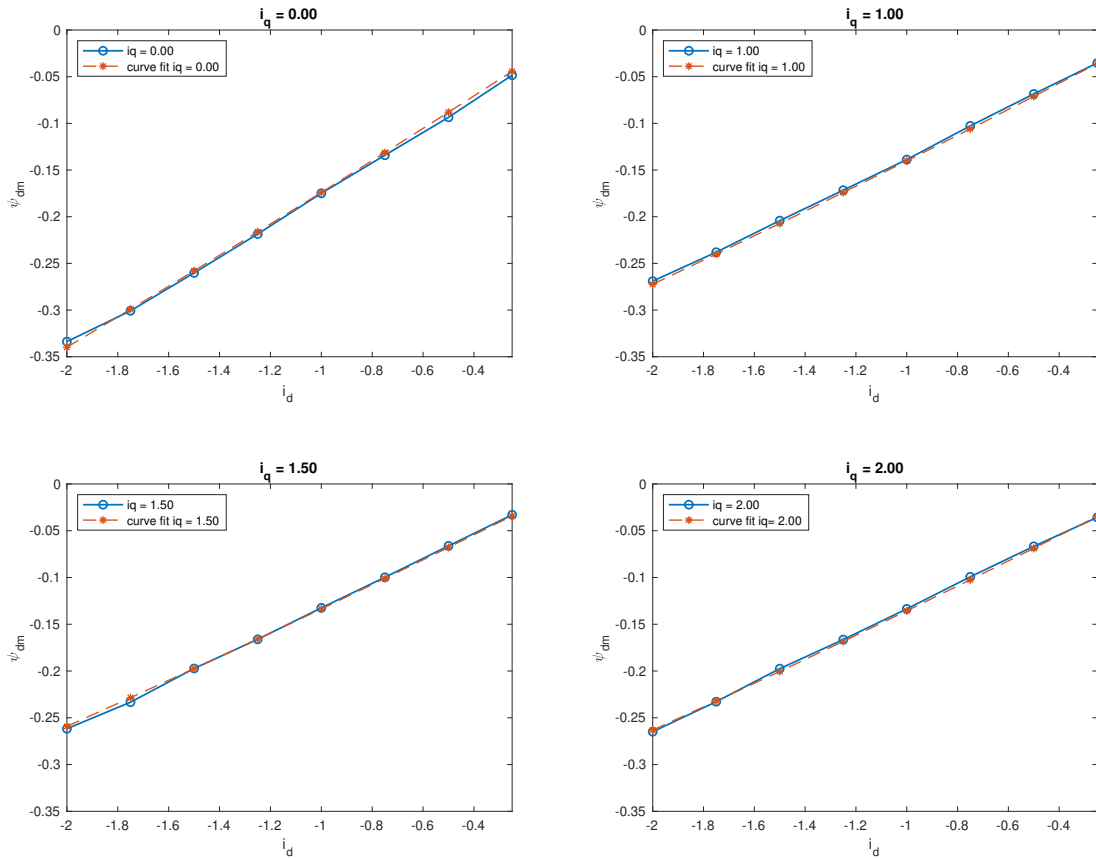
Figure 22: Stumberger data, flux linkage fit to 55

Curve Fit: $\psi_q = 0.411\, i_q\; 0.068\, i_d\, i_q\; 0.002\, i_d^2\, i_q + -0.027\, i_d\, i_q^2\; -0.112\, i_q^2 + 0.016\, i_q^3\; 0.003\, i_d^2\, i_q$
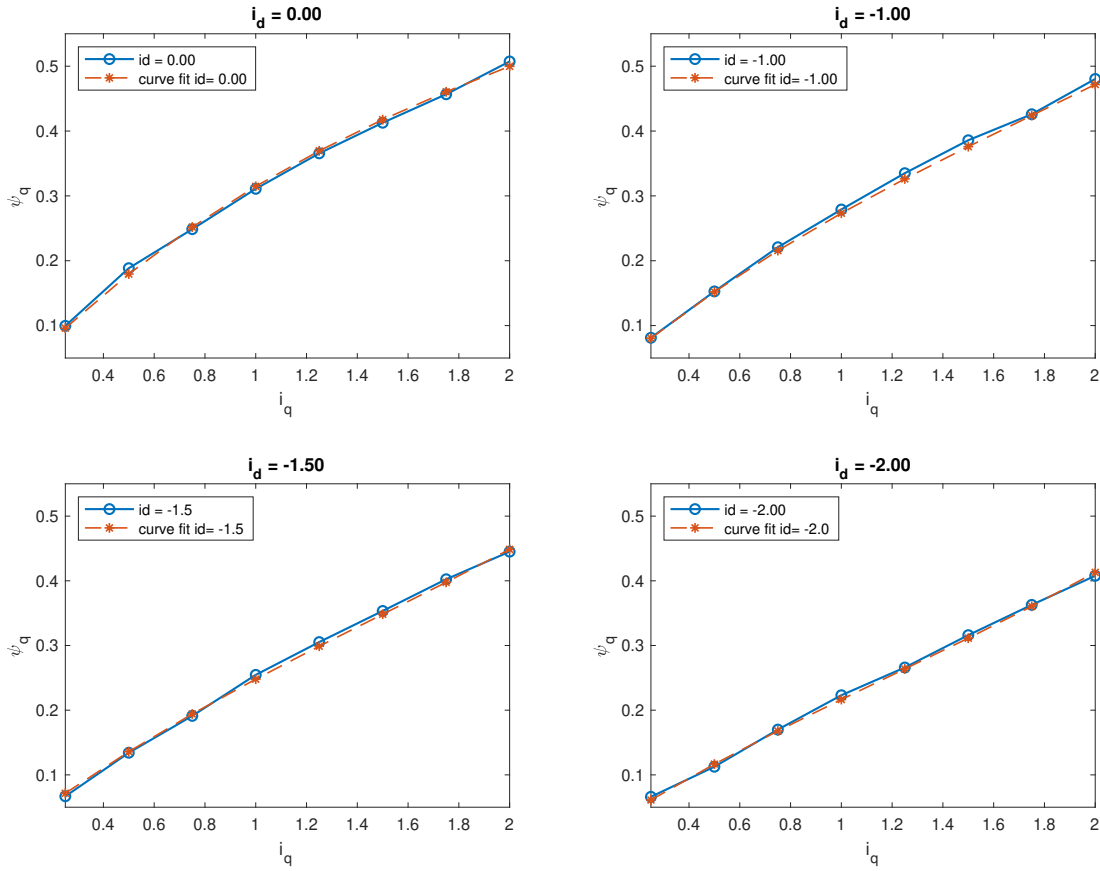
Figure 23: Stumberger data, flux linkage fit to 58

Coefficient	Value
d_{10}	0.178
d_{11}	0.045
d_{12}	0.009
d_{20}	0.004
d_{13}	0.002
rmse	0.003
adj.R^2	0.999

Table 8: Coefficients: Curve fit of Paper data flux linkage to model 6

Coefficient	value
q_{01}	0.411
q_{11}	0.068
q_{21}	0.002
q_{12}	-0.027
q_{02}	-0.112
q_{03}	0.016
q_{31}	0.003
rmse	0.006
adj.R^2	0.998

Table 9: Coefficients: Curve fit of Paper data flux linkage to model 7

4.3.1 Discussion on paper and curve fits

The curve fit to the differential inductances was very good, as can be seen in all the four plots above, and the trends are captured sufficiently. As the d- and q-axis flux linkage models were in fact not developed to fit these results specifically, it would have been reasonable that there would be some deviation here. However, the flux linkages were fitted to these models with very good goodness-of-fit statistics. The difference in coefficients from the curve fit to the inductances, to the curve fit to the flux was also quite small, especially on the d-axis, indicating that the inductance-based fit resulted in a sufficient flux model for the data. It was concluded in the Stumberger study that the reciprocal condition was not fulfilled for their data, and it is also not fulfilled for the new developed models. Still, the real value difference between the two cross-coupling differential inductances in the data is not too large relative to the size of the self differential inductances. Also the two cross-coupling inductance expressions of the new model could be somewhat overlapping and with small differences, depending on the coefficients.

4.4 Saturation and cross-coupling phenomena in study data

Both saturation and cross-coupling are visible in the digitized data and plots. On the current induced d-axis flux, in figure 22, there is clear dependence on the q-axis current. The flux linkage rate of increase, although rather steady with respect to the d-axis current, visibly decreases when higher q-axis currents are applied in 22. Note that there is a significant flux increase when the q-axis current is increased from zero at high negative d-axis currents, but the increase more or less disappears at 1 p.u. q-axis current. This can be interpreted as cross-saturation on the d-axis caused by, or increased by, the q-axis current, decreasing the d-axis reactance. Here it would be interesting to know to what degree the iron is saturated, to understand why increasing the q-axis current after 1 p.u. seemingly does not affect the reactance further.

Another interesting point here it that there is no less cross-saturation for higher negative d-axis current, rather the opposite if anything. One would expect increasing negative d-axis currents to remove saturation in the motor, but that is not visible in this plot, or in the differential self-inductance plot in figure 18b.

Next, on the q-axis, the flux linkage is very much dependent on the q-axis current, and it seems that there is cross-saturation also here, and it is even more visible on this axis. The q-axis differential self-inductance in figure 21 is at its peak when both currents are close to zero. The reactance seems to decrease for more q-axis current in 23, especially where the negative d-axis current is also high. A possible explanation is that there is saturation on the q-axis, and also quite a bit of cross-saturation from the d-axis. Again, it seems that the negative d-axis does not increase, but decreases the reactance on the path, while one could expect it to lessen the magnetic field and saturation. This is interesting for further studies. There could be several effects taking place in the same region, or perhaps some unknown factors in the motor or tests affecting the saturation.

5 New curve fits

In order to verify the new and more detailed model functions that were developed in the previous chapter, function 55 and 58, the data from the conducted lab tests were curve fitted to them. The resulting curve fit and original lab data is shown in figures 24 and 25, with the pertaining coefficient values presented in tables 10 and 11.

Coefficient	Value
d_{10}	0.329
d_{11}	-0.233
d_{12}	-0.519
d_{20}	-0.151
d_{13}	-0.068
rmse	0.027
sdjrsquare	0.976

Table 10: Coefficients from lab data curve fit to function 55

Coefficient	value
q_{01}	1.259
q_{11}	-0.051
q_{21}	-0.032
q_{12}	0.0144
q_{02}	-0.545
q_{03}	0.327
q_{31}	-0.029
rmse	0.023
asdjrsquare	0.993

Table 11: Coefficients from lab data curve fit to function 58
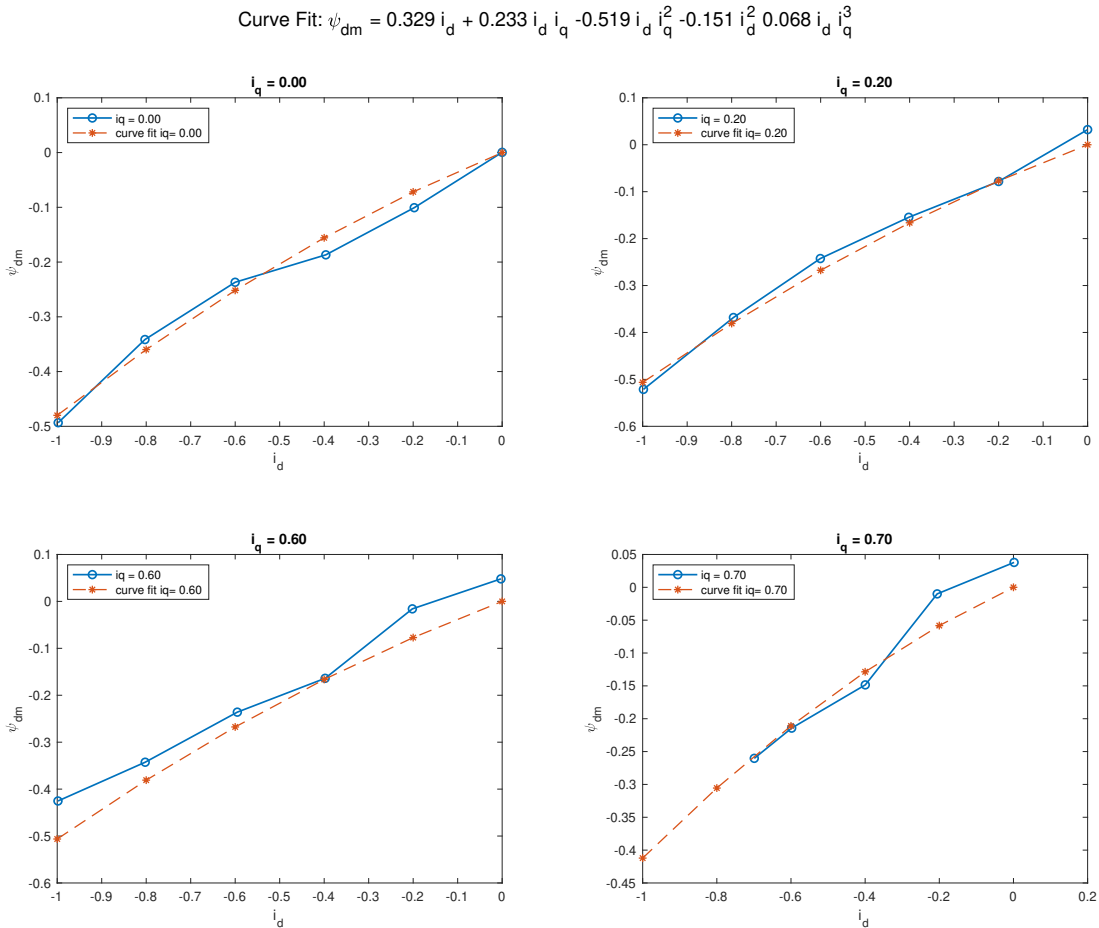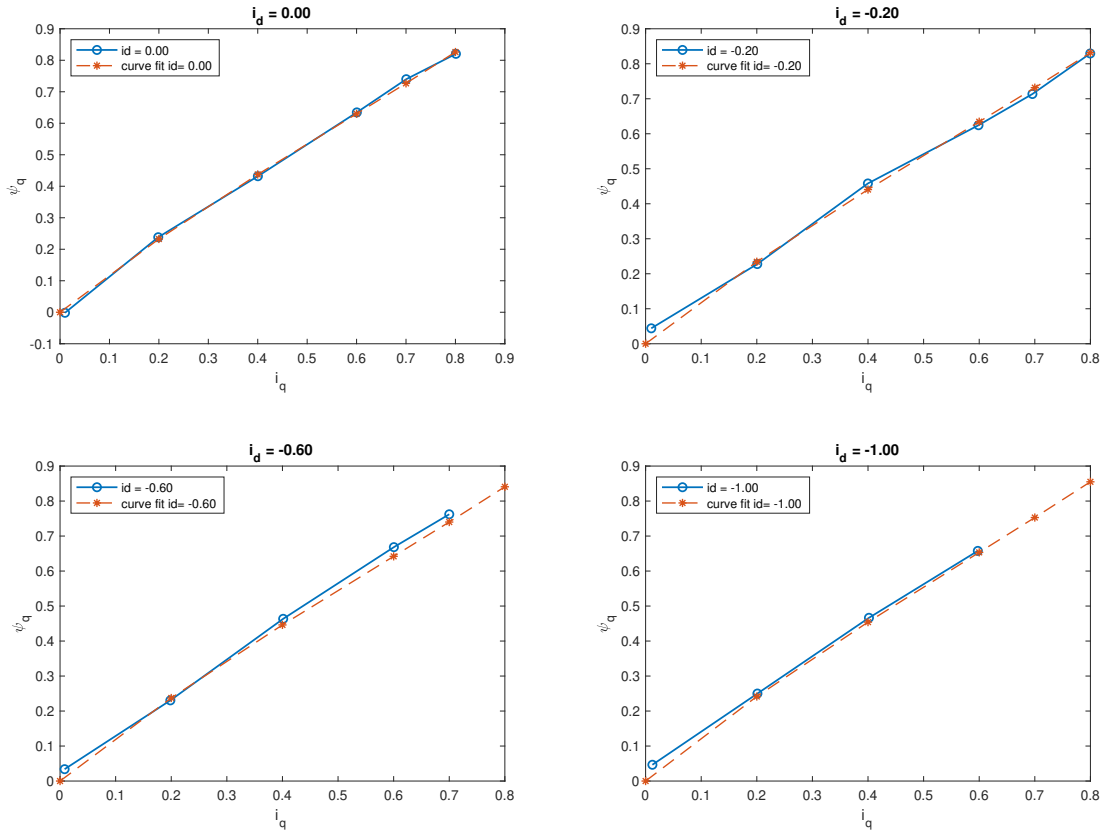

Figure 24: Lab data fitted to 55

Figure 25: Lab data fitted to 58

These curves capture the main trends in the data, but numerically, the fit is not perfect. The rmse is small, but not insignificant. The interval of 95 % confidence is however quite large for many of the coefficients, meaning that only a small error in the fitted data would change the coefficients visibly. Both numerically and visibly, the q-axis function fits better than the d-axis function. Several alterations to the model functions, including more higher-order terms, were done and evaluated to see if the curve fit would improve, but the rmse and adjusted coefficient of determination remained more or less the same.

As remarked upon previously, the data from the conducted IPMSM tests include some datapoints that deviate notably from the general trends in the dataset and causes bumps in the surface plots. This can be an explanation to why the curve fits are not better. The fact that several alterations to the models did not improve the fit indicates that the curve fit is more or less as good as possible with a polynomial model. Based on this, the curve fit results are considered sufficient. What can be noted is that the actual data of the current induced d-axis flux deviates from the curve in the area where one would expect the highest saturation, i.e. at small d-axis currents and higher q-axis currents. This could be measurement errors, but it could also be a result of saturation effects, and should be studied more closely.

Lastly, in an attempt to improve the fit and understanding of the data, there was done a curve fit of the lab data of the d-axis flux to the function in 55, but where the constant value for the PM flux was not enforced. As explained in chapter 3.2, until now a constant of 0.954 was subtracted from the d-axis flux linkage values in the lab test data in order to do curve fittings to the stator current induced part of the flux only, i.e. applying a constant PM flux value. However, now the lab dataset of the entire d-axis flux was curve fitted to the model in 55, adding a last constant term which was to be determined in the curve fitting. The result of this curve fit was an rmse of 0.022, and adjusted R squared of 0.984, which was a numerically slightly better fit compared to the results in table 10, where the PM flux was 0.954. The constant term in this curve fit was calculated to 0.984, with 95 % confidence bounds at 0.968 and 1.001. This is visibly higher than the motor data value, and could indicate that either the PM flux value or the flux linkage models are not sufficiently precise.

6 Discussion

6.1 Observations from lab tests and Stumberger paper

When comparing the lab test results with the results in the study by Stumberger (2003), it is clear that there are more interesting trends in the study results compared to the obtained lab-motor results, which are fairly linear and somewhat uniform. The flux variation from different saturation phenomena that one would possibly expect to see in the lab results were not clearly present. In the Stumberger study, there was cross-coupling and saturation effects on both axes, but particularly on the q-axis. In the lab results too, cross-coupling is notable on both axes, although minimal on the q-axis flux. The rate of increase in the d-axis flux is somewhat smaller at high q-axis currents when the d-axis current approaches zero, which can possibly be attributed to saturation. This is the area most likely to see saturation, as explained in chapter 3.3. Still, one must consider that there is some uncertainty to this hypothesis due to deviation and possible measurement errors in the datapoints. As previously explained, the Stumberger study tests were done using a locked-rotor method, and it is likely that these results are more precise than the conducted lab tests.

It is important to note that, as explained in chapter 3.2, the IPMSM test rig did only allow a limited range of stator currents and speeds. This was due to the inverter voltage restrictions, and the torque range of the IM. The consequence was that it was more difficult to come to absolutely valid conclusions with regards to the flux-current relation and saturation and cross-coupling effects, which was one of the main objectives. It is likely that more saturation phenomena would be visible at higher q-axis currents or positive d-axis currents, but the degree of this depends on the design and is complicated to predict.

The flux linkage and current data from lab testing were first fitted to the models in 45, two third-degree polynomials with flux linkage as state variables, four terms on the d-axis and five on the q-axis. This fit was quite good, but the rmse was not insignificant, and there were several datapoints on the d-axis flux that was captured badly in the model. Next the data was fitted to the two fourth-degree polynomials in equation 46, where the d- and q-axis models have two and three terms, respectively. The d-axis current model, with only two terms, resulted in a mediocre fit, while the q-axis was better. Enforcing the reciprocal condition on these two models had a small effect on the fit results. It seems likely that the conducted lab test results did not fulfill the reciprocal condition completely, but the difference between the cross-coupling inductances are not so large that it would indicate clear faults with the results. The reciprocal condition, and what would be possible explanations for why it is not fulfilled, is a topic that should be researched further.

Next, consider the different polynomial models that were curve-fitted to the study data. It is evident that deviating datapoints are difficult to capture regardless of number of higher-degree terms. However, the fourth-degree polynomials with five and seven terms that were developed from integrating inductance models, presented in 55 and 58, are sufficient in representing quite some data variation and capturing significant tendencies in the more detailed dataset from the Stumberger study. The simpler models in equations 50 and 51 do also fit the flux linkages well, but the partial derivatives here are not satisfactory compared with the data. These larger polynomial models of the d- and q-axis flux linkages also have dependence on the same axis current in all terms, including the terms that represent cross-saturation. This is a notable observation for further work. An interpretation for this could be that the cross-coupling saturation is very much dependent on the flux on the same axis, which is expected. Lastly, it was noted that the flux linkage curves based on differential-inductance fitted coefficients gave satisfactory results in chapter 4.3. It seems that this could be a good approach to including the more detailed tendencies of the differential inductances in the flux models further on. Naturally, there are some drawbacks to this approach, for instance quite precise and smooth differential inductance data is required.

6.2 Variable PM flux linkage

During much of the curve fitting and analysis, there has been an assumption that while the stator current induced part of the d-axis flux, ψ_{dm} varies, the PM flux linkage in the d-axis, ψ_m, is constant. However, this is unlikely in reality, since also the flux from the PM is affected by magnetic saturation, which was outlaid in chapter 2. The PM magnetic field is dependent on its surroundings, so when the iron along the d-axis is saturated and the reluctance in the surrounding materials consequently increases, the PM magnetic field decreases. This is represented by an inner flux source and an inner reactance which in this case will decrease. However, although the PM flux is likely to vary depending on stator currents, it is difficult to separate this PM flux change from the variation in the stator induced flux on the d-axis, which it is known that very much depends on the currents.

Using a constant PM flux in the data processing likely affected the results to some degree. Since the lab data in this thesis is all in the second quadrant, the d-axis stator current contributed to weakening the flux on the d-axis. This means that saturation effects on the PM flux are likely more visible for current values closer to zero. Since the positive q-axis current contributes to increased flux on the d-axis path, there is likely more saturation for higher q-axis currents. In this case, the fictitious PM inner reactance and the PM flux would decrease.

When the lab result data was handled, a constant value PM flux was subtracted to find the stator current induced flux linkage. However, as explained, it is likely that this value was not constant. In the case described above, the subtracted value would be larger than the actual flux, and the processed current induced flux value would be too small compared to the actual value. There is therefore a possibility that the current induced d-axis flux in this saturated area is even higher than plotted. At the same time, the saturation would affect the current induced axis flux itself, because of the increased reluctance. In this case, several effects would be happening around the same region; a too low calculated stator current induced flux because of decreased PM flux, and a decrease in the measured d-axis flux because of saturation. It is however difficult to separate different phenomena from each other without any more information or data, and so it is not possible to conclude on this properly for now.

There was also done a curve fit to the models in equations 55 and 58, but where the d-axis data was fitted to the model, and a constant term was added, which was also to be determined by the fitting algorithm. The resulting fit was even better, but the constant term was determined to be 0.984, which is significantly higher than the expected constant term of 0.954 from the motor data. It is interesting to note that the constant term that gives the best curve fit is not equal to the value from the data. This could be an indication that the value is in fact not constant for the entire testing range. In the previous curve fittings, the possible variation in the PM flux would have had to be captured in the other current dependent terms in the models. This does, however, not necessarily imply that the actual PM flux value is higher than originally known, it may also be that the current induced d-axis flux curve simply is modeled better with a constant term in the expression. Either way, the PM flux remains a very interesting topic of further study.

Next, consider the Stumberger paper data. As explained in chapter 4, the flux linkages were obtained by integrating the stator voltage and current times the stator resistance. It follows from this method that any constant term in the flux is not included unless other tests are done to find it. In chapter 4, there were developed flux linkage models that depended on the d- and q-axis currents, meaning that it was not taken into account that some of the d-axis flux tendencies could be a consequence of a varying PM flux on the d-axis.

It would be very relevant to include the varying PM flux in further models, for instance by substituting the PM with a reactance in parallel with a current source, as presented in chapter 2. However, there is the challenge of several new unknown variables being introduced. As explained in chapter 2, the base-values are defined such that the fictitious inner PM reactance and the magnetizing reactance have the same p.u. value. In equation 35 below, also introduced in the theory chapter, there are three unknown variables; $x_{s\sigma d}$, x_{md} and i_f. The first can be removed by setting stator currents to zero and measuring the flux, as shown in equation 59. However, this is not enough, as there still are two unknown variables.

$$\psi_d(i_d, i_q) = x_{s\sigma d}(i_d, i_q)i_d + x_{md}(i_d, i_q) \cdot (i_d + i_f) \tag{35}$$

$$\psi_d(0, 0) = x_{md}(0, 0) \cdot (i_f) \tag{59}$$

One possible approach to estimate all these three values, is to keep the q-axis current at zero, but apply very small d-axis currents, so the first term remains and there are more datapoints with flux and current values to use. At least three equations are needed to obtain the unknown variables. What would be essential here, however, is that the variables have to be equal in all the equations. When there is saturation on the d-axis and the reluctance on the main flux path across the air-gap increases, the leakage flux is altered, meaning the reactance representing the flux leakage is also changed. As explained previously, the inner PM reactance is also changed if there is saturation on the d-axis. In other words, both reactances in equation 35 are dependent on stator currents. Therefore, the d-axis current have to be kept very small, so there is a good certainty that no saturation appears and affects the reactance values. Later, when the fictitious inner PM current is found, it is possible to study more in detail how the reactances depend on both stator currents.

$$\psi_d(i_{d_1}, 0) = x_{s\sigma d} \cdot (i_{d_1}, 0)i_{d_1} + x_{md}(i_{d_1}, 0) \cdot (i_{d_1} + i_f)$$
$$\psi_d(i_{d_2}, 0) = x_{s\sigma d} \cdot (i_{d_2}, 0)i_{d_2} + x_{md}(i_{d_2}, 0) \cdot (i_{d_2} + i_f)$$
$$\psi_d(i_{d_3}, 0) = x_{s\sigma d} \cdot (i_{d_3}, 0)i_{d_3} + x_{md}(i_{d_3}, 0) \cdot (i_{d_3} + i_f)$$

6.3   Saturation and cross-coupling in iron teeth

Another proposition is that a negative d-axis current will lead to a small shift of the flux space vector toward more negative d-axis flux, or a larger rotor angle, compared to the ideal motor model. In the same way, a positive d-axis current will shift the space vector toward a more positive d-axis flux, or smaller rotor angle.

The explanation for this is that if one looks inside each of the stator teeth, the stator windings will each produce a B-field, which has a direction around the coil according to the right-hand rule. This is illustrated in figure 26. On one side, the coil's own induced B-field will point in the same direction as the magnetic field coming into the stator teeth across the air-gap, while on the other side it will point the opposite direction of the incoming field. Therefore, there will be a higher total magnetic flux density on one side, moving the iron toward more saturation and increasing the reluctance.
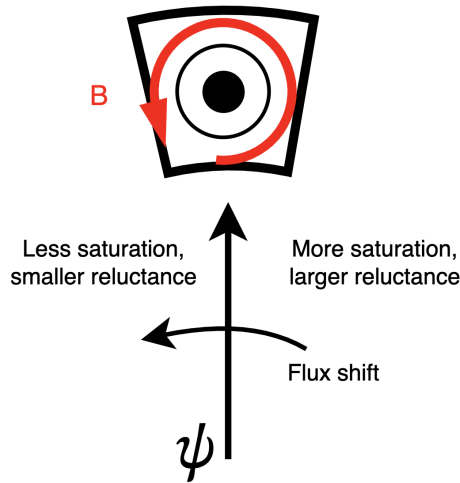

Figure 26: Illustration of saturation and flux shift in stator teeth

The magnetic flux will always follow the path of the smallest reluctance or effective air gap. Therefore the flux vector is shifted to the right or left depending on the direction of the winding current. Remember that the q-axis flux is orthogonal to the d-axis windings and the opposite, so this would clearly be a cross-coupling phenomenon. Generally, there will be set up magnetic fields around each coil in the motor. However, the strength of the field depends on the current strength, and the effect will be more visible on the fluxes if the iron on the axis is already starting to become saturated.

One could try to see these shifts in the flux plots, but it would be very difficult to separate this effect from other saturation which will be present. However, combining such an analysis with magnetic field calculations could be useful. This will have to be explored in further research.

One important consideration in all these analyses is that the flux path and saturation phenomena very much depend on the motor design. The rotor configuration, air-gap length, choice of PM and iron metal, teeth, slots etc. will all affect how the magnetic circuit turns out. Therefore it is not sufficient to observe one motor.

7 Conclusion

The main purpose of the current thesis was to explore saturation and cross-coupling phenomena in IPMSMs, and to evaluate and further develop nonlinear mathematical models of flux linkage. Lab tests of a 6-phase machine were conducted, and the results were applied to existing nonlinear models from previous master's thesises, in order to examine them. In addition, data from a previous study was analyzed and modeled, with the aim of developing more nonlinear mathematical models and detect saturation phenomena. New models were proposed and curve fitted to the obtained lab data, resulting in satisfactory fits and by that confirming the functionality of the models.

The IPMSM lab test results did not provide any significant new insight into the understanding of cross-coupling or saturation phenomena. The flux linkage observed in the conducted lab test results appeared fairly linear, making it challenging to identify saturation with certainty. However, significant saturation was observed in the data of the previously conducted study by Stumberger(2003). Also, several hypothesis were put forward regarding where in the motor saturation and cross-coupling effect would be likely, for future research. Next, it was also found that many different mathematical polynomials can model the flux linkage satisfactorily, and that developing flux linkage models based on modeling of the differential inductances could be a promising approach going forward.

The primary contribution of this study relates to the modeling of cross-coupling and saturation. However, due to the small observation of these phenomena in the conducted lab test, the contribution to the understanding of the cross-coupling and saturation phenomena is limited. The relatively small range of currents evaluated could be one of the main reasons for the limited findings.

Several components within the lab setup imposed constrains on the range of possible currents to be evaluated. The inverters' output voltage was limited significantly as to not enter too far into overmodulation based on the set DC-source voltage. This, along with limitations on the connected Induction Motor maximum torque, resulted in a fairly narrow range of testing dq-currents. Also, the results were affected by quite a few deviating datapoints, making the analysis more difficult and causing any possible findings to come with some uncertainty. Another limitation is that the analysis of saturation based solely on flux linkage-to-current mapping is not sufficient to conclude confidently, especially on more specific saturation phenomena where several effects could take place at the same time.

8 Further work

There are several research topics that would be interesting to study further based on the findings in this thesis.

First, in order to further validate the nonlinear models proposed, more work is needed. Applying the models to other comparable set of data could contribute to this, revealing any possible shortcomings. Also, if satisfactory, these models could hopefully be used to implement an improved sensorless control system on the IPMSM.

One natural next step in understanding the cross-coupling and saturation in the tested IPMSM, would be to do complete calculations of the magnetic field in the machine. The magnetic field distribution in the motor should be measured or estimated, and it should be analyzed together with mappings of flux linkage and current. In this way, it would hopefully be possible to connect the saturation phenomena from field calculations to the flux linkages mapped with current, and therefore verify different phenomena with greater certainty.

More specifically, one possible subject of focus could be to research whether the the stator teeth flux shift that was described in the discussion, is visible in field distribution plots. If it is possible to observe this, one should see at what currents it appears, and then compare it to the mappings or flux linkage models and analyze whether the hypothesis holds and under what conditions.

Another recommendation would be to do experiments and identify PM flux linkage or fictitious current and reactance, as proposed in more detail in chapter 6.2. As the PM flux linkage is essential to the motor operation, studying the variation here due to saturation and cross-coupling could possibly be quite rewarding. After identifying the varying PM parameters, this should be implemented into the motor models, which can possibly make the models even more precise.

Next, was an assumption throughout the thesis that the z1-z2 subspace windings did not cause cross-coupling saturation in the d- and q-axis. However, although there is no electromechanical energy conversion in this subspace, there is flux linkage. A thorough literature search could possibly reveal whether this assumption is likely to hold. Dependent on this, it could be relevant to research the possible cross-coupling effects between these subspaces. Lastly, the reciprocal condition should be studied more closely. If the condition is not fulfilled in the actual motor results, it could mean that there are losses in the motor not accounted for, or that there are other shortcomings in the motor models which should be identified.

References

1. Krokeide, N. *Emulation of the cross-coupling effect in PMSMs* Project thesis (Norwegian University of Science and Technology, 2023).

2. Klyve, Ø. S. *Magnetic Modelling of Saturated IPMSMs, for Improved Torque Estimation and Accurate MTPA Control* Master thesis (Norwegian University of Science and Technology, 2021).

3. Perera, A. *Enhanced Sensorless Control of Electric Drivetrains for Deep-Sea Mining Vehicles* PhD thesis (Norwegian University of Science and Technology, 2023).

4. Mikami, H., Ide, K., Shimizu, Y., Senoo, M. & Seki, H. Historical evolution of motor technology. *Hitachi Review* **60,** 39 (2011).

5. Pellegrino, G., Boazzo, B. & Jahns, T. M. Plug-in Direct-Flux Vector Control of PM Synchronous Machine Drives. *IEEE Transactions on Industry Applications* **51,** 3848–3857 (2015).

6. Stumberger, B., Stumberger, G., Dolinar, D., Hamler, A. & Trlep, M. Evaluation of saturation and cross-magnetization effects in interior permanent-magnet synchronous motor. *IEEE Transactions on Industry Applications* **39,** 1264–1271 (2003).

7. D P Kothati, I. J. N. *Electric Machines, Fourth Edition* (Tata McGraw Hill Education Private Limited, 2010).

8. Hanselman, D. *Brushless Permanent Magnet Design, Second Edition* (Magna Physics Publishing, 2006).

9. Ba, X., Gong, Z., Guo, Y., Zhang, C. & Zhu, J. Development of Equivalent Circuit Models of Permanent Magnet Synchronous Motors Considering Core Loss. *Energies* **15** (2022).

10. Jaszczolt, C. *Understanding Permanent Magnet Motors* https://www.controleng.com/articles/understanding-permanent-magnet-motors/. Accessed: 17.12.2022.

11. Nilsen, R. *TET4120 Electric Drives* (Department of Electric Power Engineering, Norwegian University of Science and Technology, 2018).

12. Zhao, Y. & Lipo, T. Space vector PWM control of dual three-phase induction machine using vector space decomposition. *IEEE Transactions on Industry Applications* **31,** 1100–1109 (1995).

13. Nilssen, R. *Vizualisation of Electrical Machines* 2023.

14. Li, Z. & Li, H. *MTPA control of PMSM system considering saturation and cross-coupling* in *2012 15th International Conference on Electrical Machines and Systems (ICEMS)* (2012).

15. Hinkkanen, M. e. a. Sensorless Self-Commissioning of Synchronous Reluctance Motors at Standstill Without Rotor Locking. *IEEE Transactions on Industry Applications* **53** (2017).

16. Uosef, A. A. H. *Sensorless Control of Six-Phase Permanent Magnet Synchronous Machines* Master thesis (Norwegian University of Science and Technology, 2023).

Appendix

Coefficient	Value
d_{10}	2.072
d_{13}	1.284
$1/d_{10}$	0.483
rmse	0.078
adjrsquare	0.946

Table 12: Coefficients from curve fit of lab data to 46, flux as s.v. reciprocal condition not fulfilled
*This value has a very large confidence bounds

Coefficient	Value
q_{01}	0.878
q_{03}	0.137
q_{22}	-0.362*
$1/q_{01}$	1.139
rmse	0.021
adjrsquare	0.994

Table 13: Coefficients from curve fit of lab data to 46, flux as s.v. reciprocal condition not fulfilled
*This value has a very large confidence bounds

Coefficient	Value
d_{10}	0.473
d_{11}	0.024
d_{02}	-0.228*
q_{12}	-0.452*
rmse	0.025
adjrsquare	0.979

Table 14: Coefficients from curve fit of lab data to 45, current as s.v. reciprocal condition not fulfilled
*This value has a very large confidence bounds

Coefficient	Value
q_{01}	1.184
q_{02}	-0.195
d_{11}	0.075
d_{02}	0.064
q_{12}	-0.161
rmse	0.020
adjrsquare	0.995

Table 15: Coefficients from curve fit of lab data to 45, current as s.v. reciprocal condition not fulfilled
*This value has a very large confidence bounds